Article:
del Signore, Steven J, Biber, Sarah A, Lehmann, Katherine S et al. (5 more authors) (2017) dOCRL maintains immune cell quiescence in Drosophila by regulating endosomal traffic. PLoS Genetics. ISSN 1553-7404

https://doi.org/10.1371/journal.pgen.1007052

PLOS Genetics

dOCRL maintains immune cell quiescence in Drosophila by regulating endosomal traffic

--Manuscript Draft--

Manuscript Number:	PGENETICS-D-17-00662
Full Title:	dOCRL maintains immune cell quiescence in Drosophila by regulating endosomal traffic
Short Title:	dOCRL restricts immune activation in Drosophila
Article Type:	Research Article
Section/Category:	General
Keywords:	Drosophila; OCRL; Lowe Syndrome; endosome; Toll; innate immunity
Corresponding Author:	Avital Rodal Brandeis University Waltham, UNITED STATES
Corresponding Author's Institution:	Brandeis University
First Author:	Steven J Del Signore
Order of Authors:	Steven J Del Signore
	Sarah A Biber
	Katherine S. Lehmann
	Tania L Eskin
	Sean T Sweeney
	Avital Rodal
Abstract:	Lowe Syndrome is a developmental disorder characterized by eye, kidney, and neurological pathologies, and is caused by mutations in the phosphatidylinositol-5-phosphatase OCRL. OCRL plays diverse roles in endocytic and endolysosomal trafficking, cytokinesis, and ciliogenesis, but it is unclear which of these cellular functions underlie specific patient symptoms. Here, we show that mutation of Drosophila OCRL causes cell-autonomous activation of hemocytes, which are cells of the innate immune system. Among many cell biological defects in docrl mutant hemocytes, we pinpointed the cause of innate immune activation to reduced Rab11-dependent recycling traffic and concomitant amplification of Rab7-dependent late endosome traffic. Activation is associated with mis-sorting of the Toll ligand Spätzle, excessive secretion of Spätzle into hemolymph, and Toll pathway activation. Thus, docrl regulation of endosomal traffic maintains innate immune cells in a poised, but quiescent state, suggesting mechanisms by which endosomal misregulation of signaling may contribute to symptoms of Lowe syndrome.
Suggested Reviewers:	Jonathan Kagan Children's Hospital Boston jonathan.kagan@childrens.harvard.edu Innate Immunity
	Neal Silverman University of Massachusetts Medical School Neal.Silverman@umassmed.edu Innate Immunity in Drosophila
	Martin Lowe University of Manchester martin.p.lowe@manchester.ac.uk Lowe Syndrome cell biology
	Pete Cullen University of Bristol Faculty of Health Sciences

	pete.cullen@bristol.ac.uk Endosomal traffic
	Arnaud Echard Institut Pasteur arnaud.echard@pasteur.fr Lowe Syndrome Cell Biology
Opposed Reviewers:	
Additional Information:	
Question	**Response**
Financial Disclosure Please describe all sources of funding that have supported your work. **This information is required for submission and will be published with your article, should it be accepted.** A complete funding statement should do the following: Include **grant numbers and the URLs** of any funder's website. Use the full name, not acronyms, of funding institutions, and use initials to identify authors who received the funding. **Describe the role** of any sponsors or funders in the study design, data collection and analysis, decision to publish, or preparation of the manuscript. If the funders had **no role** in any of the above, include this sentence at the end of your statement: "*The funders had no role in study design, data collection and analysis, decision to publish, or preparation of the manuscript.*" However, if the study was **unfunded**, please provide a statement that clearly indicates this, for example: "*The author(s) received no specific funding for this work.*" * typeset	Stocks and reagents were obtained from the Bloomington Drosophila Stock Center (NIH P40OD018537), the Drosophila Genetics Resource Center (NIH 2P40OD010949-10A1), and the Developmental Studies Hybridoma Bank. This work was supported by the Lowe Syndrome Association (A.A.R.), National Institutes of Health T32 NS007292 (S.J.D), and Medical Research Council (UK) MR/M013596/1 (STS). The funders had no role in study design, data collection and analysis, decision to publish, or preparation of the manuscript.
Competing Interests You are responsible for recognizing and disclosing on behalf of all authors any competing interest that could be perceived to bias their work, acknowledging all financial support and any other relevant financial or non-financial competing interests. Do any authors of this manuscript have competing interests (as described in the PLOS Policy on Declaration and	The authors have declared that no competing interests exist.

Evaluation of Competing Interests)? **If yes**, please provide details about any and all competing interests in the box below. Your response should begin with this statement: *I have read the journal's policy and the authors of this manuscript have the following competing interests:* **If no** authors have any competing interests to declare, please enter this statement in the box: "*The authors have declared that no competing interests exist.*" * typeset	
Data Availability PLOS journals require authors to make all data underlying the findings described in their manuscript fully available, without restriction and from the time of publication, with only rare exceptions to address legal and ethical concerns (see the PLOS Data Policy and FAQ for further details). When submitting a manuscript, authors must provide a Data Availability Statement that describes where the data underlying their manuscript can be found. Your answers to the following constitute your statement about data availability and will be included with the article in the event of publication. **Please note that simply stating 'data available on request from the author' is not acceptable. *If, however, your data are only available upon request from the author(s), you must answer "No" to the first question below, and explain your exceptional situation in the text box provided.*** Do the authors confirm that all data underlying the findings described in their manuscript are fully available without restriction?	Yes - all data are fully available without restriction
Please describe where your data may be found, writing in full sentences. **Your answers should be entered into the box below and will be published in the form you provide them, if your manuscript is accepted.** If you are copying our sample text below, please ensure you replace any instances of XXX with the appropriate details.	All relevant data are within the paper and its Supporting Information files.

If your data are all contained within the paper and/or Supporting Information files, please state this in your answer below. For example, “All relevant data are within the paper and its Supporting Information files.” If your data are held or will be held in a public repository, include URLs, accession numbers or DOIs. For example, “All XXX files are available from the XXX database (accession number(s) XXX, XXX)." If this information will only be available after acceptance, please indicate this by ticking the box below. If neither of these applies but you are able to provide details of access elsewhere, with or without limitations, please do so in the box below. For example: “Data are available from the XXX Institutional Data Access / Ethics Committee for researchers who meet the criteria for access to confidential data.” “Data are from the XXX study whose authors may be contacted at XXX.” * typeset	
Additional data availability information:	

Cover Letter

Brandeis University
Avital A. Rodal, PhD
Assistant Professor
Biology Department
Rosenstiel Basic Medical Sciences Research Center
415 South Street, Mailstop 029
Waltham, Massachusetts 02454-9110
Email: arodal@brandeis.edu

3/31/17

Dear editors,

We are submitting our manuscript, entitled '**dOCRL maintains immune quiescence by regulating endosomal traffic**', by Del Signore et al. for consideration as an article in *PLOS Genetics*. Lowe Syndrome is a congenital disease characterized by severe brain, eye, and kidney pathologies, and is caused by mutations in the phosphoinositide 5-phosphatase OCRL. Though *in vitro* studies have identified diverse roles for OCRL in ciliogenesis, endocytosis, endosomal trafficking, and cytokinesis, it has remained a mystery which of these cell biological processes contribute to specific symptoms in Lowe Syndrome patients, and how this leads to tissue and organ-level defects in disease.

In the attached manuscript, we use *Drosophila* to perform the first *in vivo* mechanistic cell biological studies to illuminate the specific contributions of OCRL cellular functions to organism-level physiology. Surprisingly, we found that mutation of the *Drosophila* OCRL homolog *docrl* caused a profound activation of the innate immune system. This phenotype had previously been observed in several endosomal trafficking mutants, but it has remained unclear which immune cells and tissues contribute to this phenotype, and which endosomal trafficking steps and immune-related cargoes are involved. Here, we show that the *docrl* phenotype is cell autonomous to macrophage-like hemocytes, and among diverse trafficking phenotypes in these cells, we were able to ascribe immune activation specifically to defective late/recycling endosomal transport, associated with mis-sorting of the immune-stimulating Toll ligand Spz. Our results are particularly intriguing in light of recent studies in mammals that implicate Toll-like signaling in astrocyte-mediated inflammation and seizure susceptibility, which is a significant neurological symptom of Lowe Syndrome. Overall, our findings define novel mechanisms by which membrane traffic controls a conserved signaling pathway, show that tissue-level defects in a pleiotropic disease like Lowe Syndrome can be linked to specific cell biological processes, and open a new avenue of investigation into Lowe Syndrome pathogenesis.

We believe that our findings should be of broad interest to cell and developmental biologists working on membrane traffic, signaling and innate immunity. We know of no financial or other conflicts of interest influencing our results. None of the data have been submitted to another journal for publication. We recommend the following reviewers with expertise in the areas of OCRL function, membrane trafficking, and immune activation:

Jon Kagan	jonathan.kagan@childrens.harvard.edu
Neal Silverman	Neal.Silverman@umassmed.edu
Martin Lowe	martin.p.lowe@manchester.ac.uk
Pete Cullen	pete.cullen@bristol.ac.uk
Arnaud Echard	arnaud.echard@pasteur.fr

Thank you again for considering our manuscript.
Best regards,

Avital A. Rodal

dOCRL maintains immune cell quiescence by regulating endosomal traffic

Steven J. Del Signore[1¶], Sarah A. Biber[1¶], Katherine S. Lehmann[1], Tania L. Eskin[1], Sean T. Sweeney[2], and Avital A. Rodal[1,*]

[1]Rosenstiel Basic Medical Sciences Research Center, Department of Biology
Brandeis University, Waltham, MA 02453

[1]Department of Biology, University of York, York YO10 5DD, UK.

¶co-first authors

*Corresponding author:
Avital A. Rodal
Rosenstiel Basic Medical Sciences Research Center
Brandeis University
Tel. 781-736-2459
Email: arodal@brandeis.edu

ABSTRACT

Lowe Syndrome is a developmental disorder characterized by eye, kidney, and neurological pathologies, and is caused by mutations in the phosphatidylinositol-5-phosphatase OCRL. OCRL plays diverse roles in endocytic and endolysosomal trafficking, cytokinesis, and ciliogenesis, but it is unclear which of these cellular functions underlie specific patient symptoms. Here, we show that mutation of *Drosophila* OCRL causes cell-autonomous activation of hemocytes, which are cells of the innate immune system. Among many cell biological defects in *docrl* mutant hemocytes, we pinpointed the cause of innate immune activation to reduced Rab11-dependent recycling traffic and concomitant amplification of Rab7-dependent late endosome traffic. Activation is associated with mis-sorting of the Toll ligand Spätzle, excessive secretion of Spätzle into hemolymph, and Toll pathway activation. Thus, *docrl* regulation of endosomal traffic maintains innate immune cells in a poised, but quiescent state, suggesting mechanisms by which endosomal misregulation of signaling may contribute to symptoms of Lowe syndrome.

KEY WORDS

OCRL, Lowe Syndrome, phosphoinositide, hemocyte, innate immunity, Toll, Spz, *Drosophila*, endosome

INTRODUCTION

Lowe syndrome is an X-linked disorder caused by mutations in the phosphoinositide-5-phosphatase OCRL (**O**culo**c**ereb**r**orenal Syndrome of **L**owe). Lowe Syndrome patients display renal proximal tubule dysfunction, glaucoma, cataracts, and neurological phenotypes such as cognitive and behavioral impairments, hypotonia, and epilepsy [1]. OCRL encodes a 901 amino acid protein with an N-terminal Pleckstrin Homology (PH) domain bearing clathrin-binding motifs, a central phosphoinositide-5-phosphatase domain (with preference for $PI(4,5)P_2$ and $PI(3,4,5)P_3$), as well as an ASPM-SPD2-hydin (ASH) domain and a catalytically inactive Rho GTPase activating (RhoGAP) domain that each mediate interactions with membrane-associated proteins such as Rab GTPases, IPIP27A/B, and APPL [2]. OCRL localizes to multiple membrane compartments and is involved in a range of cell biological processes, including clathrin-mediated endocytosis [3-5], intracellular trafficking [6-9], actin cytoskeleton regulation [5, 10, 11], ciliogenesis [12], and cytokinesis [10, 13]. However, it remains unclear precisely how these diverse cellular requirements contribute to tissue and organ level pathology in Lowe Syndrome patients. A redundant gene, INPP5B, may partially compensate for loss of OCRL, complicating studies in vertebrate systems [12, 14, 15]. By contrast, *Drosophila* expresses only a single homolog of OCRL, CG3573/dOCRL [13], and may therefore be a useful model for understanding the functions of OCRL in complex tissues *in vivo*. dOCRL is required for cytokinesis in cultured S2 cells [13], but its functions have not yet been examined *in vivo*.

Membrane traffic plays critical roles in regulating signal transduction in many developmental contexts. Signaling cargoes, including both ligands and receptors, are rapidly trafficked through the endocytic system, changing their signaling activities en route [16]. Therefore, mis-regulation of membrane trafficking pathways can lead to drastic alterations in signal output. In *Drosophila*, the innate immune system is poised to

respond quickly and effectively to infection. Mutants in a variety of components of the endosomal trafficking system exhibit hyperactivation of the immune response and increased hemocyte abundance [17-21], but it has remained unclear which specific immune tissues or pathways are altered or how this leads to hemocyte activation. Here we show that dOCRL controls endosomal traffic in *Drosophila* larval hemocytes to restrict Toll-associated innate immune activation.

RESULTS

docrl is required to maintain immune quiescence

To investigate the role of dOCRL *in vivo*, we generated null alleles by excision of a P element from the viable, fertile line *docrl*^{EY15890} (**Fig S1A**) and isolated two null alleles, *docrl*$^{\Delta 3}$ and *docrl*$^{\Delta 4}$, which lacked the dOCRL protein product, and were larval or pupal lethal when homozygous (**Fig S1B,C**). Lethality was specific to *docrl*, as it was not complemented by a deficiency removing the *docrl* locus, and was rescued by a *docrl*-containing genomic fragment (**Fig S1C**). Upon dissecting *docrl* mutant larvae, we observed a striking (5-10 fold) increase in the numbers of circulating hemocytes (**Fig 1A-B**), which are macrophage-like cells that mediate innate immune responses. Notably, *docrl*$^{\Delta 3}$ larvae still accumulated excess hemocytes and died as larvae and pupae when raised under axenic conditions (**Fig S1C**), suggesting that immune activation was not due to over-sensitivity to pathogens. *docrl* mutants exhibited few actively dividing cells (marked by phosphorylated histone H3, **Fig S2A**), suggesting that excess hemocytes do not arise from increased cell division, but instead may reflect reduced hemocyte turnover [22]. Though we detected cytokinetic defects in *docrl* mutant hemocytes (**Fig S2B-C**), as previously described in cultured cells [10, 13], this appeared to be insufficient to counteract the excess hemocyte phenotype. Finally, both a *docrl*-containing genomic fragment and GAL4-UAS-driven dOCRL-EGFP restored hemocyte numbers to control levels, indicating that this phenotype is specific to loss of *docrl* (**Figs. 1A,B**).

We also observed the frequent presence of large melanotic masses in the posterior larval body cavity (**Fig 1C-D**). Such masses often occur in mutants with excess hemocytes, due to encapsulation of self-tissue in the absence of infection [23].

To test if this was the case in *docrl* mutants, we visualized genetically marked hemocytes (He-GAL4 driving UAS-GFP.nls) directly through the cuticles of live larvae. Melanotic masses were indeed surrounded by GFP-positive blood cells (**Fig 1E**). However, excess hemocytes were observed in *docrl* mutant larva with or without melanotic masses, suggesting that the underlying phenotype in *docrl* mutants is hemocyte over-abundance.

We next asked which of several innate immune-implicated tissues require dOCRL to limit hemocyte number: hemocytes themselves, the lymph gland (the site of hemocyte precursor maturation [24]), the fat body (which mediates the majority of antimicrobial peptide expression [25]), and nephrocytes (which mediate clearance of immune-suppressing serpins [26]). Hemocyte number was rescued cell-autonomously by driving dOCRL-eGFP (but not by control mCD8-GFP) in hemocytes with He-Gal4 (**Fig 1B,F**). By contrast, expression of dOCRL-EGFP in the fat body, with the strong driver Lsp2-GAL4, did not restore hemocyte numbers to wild type levels (**Fig 1F**). Further, expression of dOCRL-EGFP by the driver Dot-GAL4, which expresses at high levels in salivary glands, lymph gland, and nephrocytes and only at low levels in hemocytes [27], did not significantly rescue hemocyte abundance (**Fig 1F**). Therefore, dOCRL is required cell-autonomously in mature hemocytes to restrict hemocyte number.

docrl *mutants exhibit altered hemocyte differentiation and activation*

Larval hemocyte types include plasmatocytes, which are small macrophage-like cells; crystal cells, which control melanization of foreign bodies; and lamellocytes, which are large, banana-shaped cells involved in encapsulation of foreign bodies. The majority of circulating hemocytes are plasmatocytes, while lamellocytes are rare in unstimulated larvae [28]. However, when we examined hemocyte composition by immunostaining with the antibodies P1 (which labels plasmatocytes) and L1 (which labels lamellocytes), we found that 21% of hemocytes in *docrl* mutant larvae were L1-positive (**Fig 2A,B**). Surprisingly, 62% of these L1-positive cells appeared morphologically similar to plasmatocytes (**Fig 2C**), suggesting these cells may represent plasmatocytes or pro-hemocytes in the process of differentiating into lamellocytes [29]. Aberrant hemocyte

differentiation was fully rescued by a single chromosomal copy of dOCRL, but only partially rescued by expression of dOCRL-EGFP with the He-GAL4 driver (**Fig 2B**), suggesting that lamellocyte differentiation was not completely cell autonomous to He-GAL4-expressing cells, or that it may arise from the 20% of hemocytes that do not express this GAL4 driver [30].

One major feature of hemocyte activation is a dramatic increase in actin filament polymerization [17, 31]. We visualized F-actin by phalloidin staining and measured an approximately 20-fold increase in F-actin intensity in *docrl* mutants relative to controls (**Fig 2D,E**). Increased F-actin assembly corresponded to a significantly spikier morphology in *docrl* mutant hemocytes (**Fig 2F**), also consistent with hemocyte activation [31]. These cytoskeletal phenotypes were rescued cell autonomously by expressing dOCRL-EGFP with the He-GAL4 driver (**Fig 2E,F**). Together, these data indicate that hemocytes in *docrl* mutants exhibit cell autonomous hyper-activation and partially cell autonomous hyper-differentiation, in addition to greatly increased abundance.

dOCRL regulates PIP_2 homeostasis in diverse endosomal compartments

To investigate the role of *docrl* in hemocyte physiology, we examined dOCRL localization in hemocytes by live imaging of endogenously tagged dOCRL (dOCRL-TagRFPT [32]), which localized to discrete puncta at the hemocyte plasma membrane and throughout the cytoplasm (**Fig 3A**). dOCRL-TagRFPT colocalized most strongly with an He-Gal4-driven GFP tagged clathrin light chain (Clc), and moderately colocalized other compartment markers (**Fig 3B**, **S3A**), including endogenously tagged YFP-Rab5 (early endosomes), YFP-Rab7 (late endosomes), YFP-Rab11 (recycling endosomes), and He-GAL4-driven Vps35-GFP (a component of the endosomal cargo-sorting retromer complex, which has itself previously been implicated in restricting innate immune activation [17, 21]). Interestingly, dOCRL exhibited a qualitatively different pattern of association with different compartments. While dOCRL localized strongly with Clc and diffusely with Rab5 early endosomes and Rab11 recycling endosomes, it exhibited a complementary association with Vps35, and accumulated in foci on Rab7 late endosomes (**Fig 3B**, **S3A**).

To test the functional requirement for this broad distribution of dOCRL, we examined the localization of the primary dOCRL substrate PIP_2 in control and mutant hemocytes by live imaging of an mCherry-tagged PH domain of PLCδ, which specifically binds $PI(4,5)P_2$ [33]. In control hemocytes, PH-PLCδ localized at low levels to the plasma membrane and in discrete intracellular puncta (**Fig 3C, Fig S3B**). By contrast, in *docrl*$^{\Delta 3}$ mutant hemocytes, PH-PLCδ accumulated at higher levels both at the plasma membrane and in intracellular puncta. At the level of the whole cell, we observed a significant increase of mean PH-PLCδ intensity relative to control, perhaps due to stabilization of the reporter in the presence of excess PIP_2 (**Fig 3C**). To better analyze whether aberrant PIP_2 associated with a specific endosomal compartment, we compared the accumulation of PH-PLCδ to fluorescently labeled endosomal markers. Levels of PH-PLCδ were increased in all compartments examined, similar to the effect seen in whole hemocytes (**Fig 3C-D**, **Fig S3B**). Together, these data suggest that dOCRL is required to maintain PIP_2 homeostasis in diverse endosomal compartments.

To test how the dOCRL phosphatase activity contributes to its role in hemocytes, we performed rescue experiments in the *docrl* mutant using He-Gal4-mediated expression of wild-type dOCRL, a phosphatase-inactive dOCRL (dOCRL^{H469R}, corresponding to a Lowe Syndrome mutation [34]), or the dOCRL phosphatase domain alone [35]. In contrast to full-length dOCRL, which rescued hemocyte abundance (**Fig 1B,F**, **3E**), hemocyte-specific expression of either phosphatase-dead dOCRL or the phosphatase domain alone did not suppress excess hemocyte numbers (**Fig 3E**), though, based on GFP and mCherry fluorescence, they were expressed as well as the wild-type transgene and much more highly than fully rescuing, endogenously tagged dOCRL. Expression of the phosphatase domain alone partially rescued F-actin levels (**Fig 3F**), though actin still accumulated at plasma membrane ruffles and in intracellular puncta. Together, these results indicate that phosphoinositide homeostasis is required for innate immune quiescence and that the phosphatase activity of dOCRL, together with contributions from other dOCRL domains, is critically involved in this process.

dOCRL is required for normal endosomal compartment structure and function

To determine the consequences of loss of *docrl* on endosomal trafficking, we first assayed the abundance and morphology of endosomal compartments. Consistent with the broad increases in PIP_2 that we observed in *docrl* mutant hemocytes, we found defects in compartment abundance, morphology, or behavior throughout the endosomal system (**Fig 4A-B, S4A**). In control hemocytes, Clc, Rab5, and Vps35 compartments formed well-distributed medium-sized puncta, while in *docrl* mutant cells these compartments fragmented into small punctae at the cell periphery, and also densely accumulated in the perinuclear region. We also observed loss of larger Vps35-positive tubulo-vesicular structures. Further, Rab5 endosomes were less motile in $docrl^{\Delta 3}$ hemocytes than in controls (**Fig S4A**). The Rab7 compartment was strikingly enlarged in *docrl* mutant hemocytes compared to controls (**Fig 4A**)**,** and the level of endogenous Rab7 was significantly increased (**Fig 4B**). We did not detect a marked change in Rab35 compartment structure or distribution in *docrl* mutants.

To assess whether these defects in membrane compartment structure correlated with changes in function, we first examined scavenger receptor-mediated endocytosis and phagocytosis, both of which are highly dependent on membrane trafficking and are critical to the functional capacity of hemocytes [36-39]. We tested scavenger receptor-mediated endocytosis by measuring internalized maleylated BSA [40] at confocal slices through the cell interior. At all time points after pulse-chase with mBSA, *docrl* mutant hemocytes exhibited reduced internalization (**Fig 4C**). Next, we tested phagocytosis by measuring the internalization of *E. coli. docrl* hemocytes readily internalized Alexa-488-labeled *E. coli*, though there was a small but significant decrease in the mean number of bacteria internalized in the population of cells (**Fig S4C**). However, *docrl* mutants are enriched for lamellocytes (**Fig 2B**) and this cell type is less phagocytically active [28], potentially reducing the mean number of bacteria per cell. Indeed, when we excluded from our analyses the hemocytes that took up no *E. coli*, *docrl* mutants were identical to controls (**Fig S4C**). These results suggest that dOCRL is not critically required for phagocytosis in hemocytes, though they do not exclude a role in phagosome maturation.

Finally, we tested whether *docrl* mutant hemocytes exhibited defects in autolysosomal degradation. We employed a dually tagged GFP-mCherry-Atg8a, which

allows detection of both nonacidic autophagosomes (coincident mCherry and GFP) as well as acidic autolyososomes (mCherry alone, due to quenching of GFP) [41]. *docrl* mutant hemocytes exhibited an increase in mCherry-GFP co-localization, indicating a failure to fuse autophagosomes with the lysosome, as well as a marked increase in both GFP and mCherry fluorescence, suggesting either upregulation of autophagy and/or a failure of lysosomal degradation (**Fig 4D**). Thus, *docrl* is strongly required for proper regulation of autophagosome-lysosome flux in hemocytes.

Specific endosomal defects contribute to* docrl *mediated immune activation

We next explored which of these dysfunctional endolysosomal compartments could account for *docrl*-induced immune activation, by individually disrupting them in otherwise wild type animals. We first inhibited the internalization step of endocytosis, by expressing dominant negative versions of clathrin heavy chain and dynamin, as well as a temperature sensitive dynamin mutant (raised at the restrictive temperature of 29ºC, at which uptake of mBSA was blocked (**Fig S5**)). None of these manipulations caused melanotic masses or excess hemocyte abundance (**Fig 5A**). OCRL interacts with Rab35 during both early endocytosis and the abscission step of cytokinesis [3, 10]. However, we did not detect changes in immune activation following expression of activated (not shown) or dominant negative Rab35 constructs (**Fig 5A**). Finally, we found that hemocyte-specific expression of the dOCRL phosphatase domain, which does not rescue innate immune activation (**Fig 3E**), robustly rescued mBSA uptake in *docrl* mutants (**Fig 5B**). Taken together, these data indicate that defects in the internalization step of endocytosis are unlikely to account for innate immune activation in *docrl* mutants. Similarly, previous work has shown that mutants affecting canonical autophagy do not cause innate immune defects [18], suggesting that changes in autophagy that we observe in *docrl* mutants (**Fig 4D**) are unlikely to account for innate immune phenotypes.

We next tested the role of post-endocytic endosomal sorting in innate immune activation. It has previously been shown that hemocyte-specific depletion of Rab5 and Rab11 increases circulating hemocyte concentration [19], suggesting again that innate immune activation may arise from defects in sorting at these endosomes. To confirm

these results and extend the analysis to include additional Rab proteins, we expressed constitutively active or dominant negative Rab5, 7, and 11 constructs in hemocytes with he-GAL4. Inhibition of Rab5 (and to a milder degree inhibition of Rab11) each led to an increase in circulating hemocyte number (**Fig 5A**). We further hypothesized that activation of Rab7 would promote a similar increase in hemocyte number, consistent with the expanded Rab7 compartment in *docrl* mutants. Indeed, hemocyte specific activation of Rab7 also led to an increase in hemocyte number (**Fig 5A**). Thus, manipulating endosomal traffic mediated by Rab5, Rab7, and Rab11 recapitulates the *docrl* mutant phenotype.

We next tested additional components of post-endocytic endosomal sorting. Retromer mediates endosomal sorting, and is composed of a cargo-selective trimer of Vps35, Vps26, and Vps29. Vps35 mutants have previously been shown to exhibit immune activation [17, 21], and we found that mutations in Vps26 similarly caused melanotic mass formation (**Fig 5C**). Vps35 and Vps26 associate with endosomes via distinct membrane binding SNX1 containing "SNX-BAR"' or SNX3 containing complexes, likely with distinct localization and functions [42]. To clarify the requirement for retromer in innate immunity, we analyzed *snx1* and *snx3* mutants. We detected frequent melanotic masses in *snx1*, but not *snx3* larvae (**Fig 5C**), suggesting that specific loss of SNX-BAR retromer underlies immune activation in *vps35* and *vps26* retromer mutants, and supporting the model that endosomal sorting underlies innate immune defects.

Finally, we asked if hemocyte-specific manipulations of Rab5, Rab7, and Rab11 could enhance or rescue the *docrl* mutant phenotype. Expression of dominant negative Rab5 and Rab11 caused early larval lethality in *docrl* mutants, but not in controls, suggesting that docrl mutants are sensitized to defects in a Rab5-Rab11 trafficking route. Strikingly, increasing Rab11 activity by overexpressing a constitutively active transgene ($Rab11^{CA}$) significantly reduced hemocyte number toward normal levels (**Fig 5D**). However, Rab5 activation failed to rescue hemocyte abundance, suggesting that *docrl*-mediated trafficking defects may occur downstream of Rab5, but upstream of Rab11. Finally, inhibition of Rab7 activity by overexpressing a dominant negative transgene ($Rab7^{DN}$) moderately suppressed the *docrl*-dependent increase in

hemocytes. Neither Rab11^{CA} nor Rab7^{DN} rescue restored *docrl* mutant adult viability, suggesting that lethality may require more complete rescue, or that it arises from a distinct function of dOCRL. Taken together, these results suggest that the membrane trafficking defect most salient to the *docrl* innate immune phenotype is mis-direction of endosomal traffic from a Rab11-dependent route towards a Rab7-dependent route.

docrl *is required to restrict Toll signaling*

We next explored which innate immune regulatory pathway might be disrupted by endosomal mis-sorting in *docrl* mutants. Immunity in *Drosophila* is mediated by several signaling pathways, including Toll and IMD, which promote expression of various target antimicrobial peptide and signaling genes [43]. We found that the Toll targets Drs and IM1 were elevated in *docrl* mutants, while the IMD-specific target Dipt was not (**Fig 6A**). Additionally, we measured increased levels of the Toll pathway transcription factor Dorsal (Dl) (**Fig S6A**), consistent with the previously observed induction of Dl expression by Toll activity [43, 44].

We next investigated potential mechanisms by which misregulation of endosomal traffic in *docrl* mutants could lead to Toll pathway activation. We detected mild but significant differences in Toll receptor levels and distribution, using He-GAL4-driven Toll-Venus (**Fig 6B**). Further, the Toll adaptor protein MyD88, which binds PIP_2 [45] relocalized from the plasma membrane in controls to intracellular punctae in *docrl* mutants (**Fig 6C**). Finally, we examined the Toll ligand Spätzle (Spz), which is secreted by hemocytes [46], and can exert both autocrine and endocrine functions in tissues including the fat body. He-GAL4-driven Spz-GFP accumulated to greater levels, and with a more punctate distribution in *docrl* mutant hemocytes relative to controls (**Fig 6D)**. Further, we found increased levels of endogenous Spz in *docrl* mutant cell-free hemolymph (**Fig 6E**). To ask whether this excess Spz release underlies innate immune activation in *docrl* mutants, we took advantage of the rescue of excess hemocytes by Rab11^{CA}. Because Rab11^{CA} autonomously suppresses hemocyte activation, we reasoned that this rescue should also suppress the *docrl*-dependent Toll signaling defects. Indeed, we found that constitutively active Rab11 caused dramatic accumulation of Spz in enlarged intracellular compartments (**Fig 6F**). Importantly, this

increase in intracellular Spz-GFP corresponded to a decrease in secreted Spz-GFP, as assayed by Western blot of cell-free hemolymph (**Fig 6G**). Together, these data suggest that a Rab11-dependent sorting route may suppress innate immune activation by retaining Spz in the cell. This association between Rab11 rescue of the *docrl* mutant phenotype and redistribution of Spz suggest that dOCRL-dependent membrane trafficking may maintain immune quiescence by regulating the localization, abundance, and release of the Toll ligand Spz (**Fig 7**).

DISCUSSION

Here we describe a requirement for the Lowe Syndrome phosphoinositide phosphatase dOCRL in maintaining innate immune quiescence in *Drosophila*. Among the many cellular functions of dOCRL, our results suggest that innate immune activation arises from defective endosomal trafficking of Toll pathway components. These data shed new light not only on OCRL function, but also on the contribution of membrane trafficking to innate immunity, and suggest new avenues for investigating the diverse symptoms of Lowe Syndrome.

dOCRL regulates endosomal sorting to maintain immune quiescence

OCRL has been implicated in numerous membrane trafficking events, including multiple steps of endocytosis and endolysosomal traffic, autophagy, ciliogenesis, and cytokinesis [2]. It has remained an open question whether individual cell and tissue level pathologies in Lowe Syndrome emerge from defects at specific cellular locations, or from a combination of OCRL-dependent functions. Though we found that *docrl* mutant hemocytes exhibit many of these cellular defects, our data strongly suggest that endosomal membrane trafficking is the primary role of dOCRL in regulating innate immune activation. First, cytokinesis defects are unlikely to account for innate immune activation, since relatively few *docrl* mutant hemocytes fail cytokinesis (**Fig S2A**), and this would be predicted to reduce rather than increase total hemocyte number. Second, defects in the internalization step of endocytosis are unlikely to cause innate immune activation, since independently inhibiting this process via clathrin and dynamin did not increase hemocyte abundance (**Fig 5A**), and rescuing defective internalization in *docrl*

mutants using the dOCRL phosphatase domain (**Fig 5B**) did not suppress hemocyte abundance (**Fig 3E**). Third, autophagy defects are unlikely to account for innate immune activation, as canonical *atg* loss-of-function mutants do not cause a melanotic mass phenotype [18]. Instead, we found that recapitulating the trafficking defects of *docrl* mutants by manipulating retromer or endosomal Rab GTPases was sufficient to produce immune activation. Further, the converse manipulation of Rab11 and Rab7 GTPases could rescue the *docrl*-induced hemocyte phenotype. Together, our results suggest that the role of dOCRL in maintaining innate immune quiescence is most critical in post-endocytic endolysosomal traffic, and adds to a growing list of OCRL functions in these compartments [9, 47, 48].

dOCRL functions cell autonomously in hemocytes to control Toll signaling

Innate immune activation in *Drosophila* depends on cross talk among multiple tissues, including hemocytes [46], the fat body [46, 49], muscles [50], and epithelia such as the gut and epidermis [51]. Our results suggest that cell-autonomous Toll activation promotes excess hemocyte accumulation. This accumulation is not due to excessive proliferation (**Fig S2A**), and may reflect the role of Toll-Dl signaling in suppressing apoptosis via *diap1* expression [22]. Prior studies have identified a similar hemocyte-specific role for endosomal GTPases in the control of hemocyte number [19]. It remains to be determined whether immune activation in other membrane trafficking mutants, including retromer (**Fig 5C**) [17, 21] and Atg6 [18], reflect defects in hemocytes or other immune relevant tissues. Indeed, the ESCRT complex members *hrs* and *myopic* (*mop*) are both required to promote Tl signaling and to generate a normal immune response in the *Drosophila* fat body [49]. Further, defective membrane balance in the fat body, via either impaired endocytosis or increased secretion, can lead to an immune response very similar to that described here [52]. While our results do not exclude a contribution of other tissues to *docrl* mediated immune activation, our rescue experiments argue strongly that hemocytes are the initiating tissue with regard to this phenotype, and that Toll signaling is intimately implicated.

Few studies to date have investigated the role of trafficking in Toll signaling in *Drosophila* innate immunity, though mammalian Toll-like receptors are known to be

regulated at specific cellular compartments [53]. Indeed, work in mammalian cells suggests that endosomal sorting may regulate the localization of cytokine receptors to prevent spurious Toll-like receptor activation [54]. Our work suggests several nonexclusive mechanisms by which changes in endosomal trafficking in *docrl* mutant hemocytes might drive Toll-mediated immune activation. First, the Toll receptor itself localizes to endosomal compartments, and though we only observed subtle changes in its distribution in *docrl* mutants (**Fig 6B**), the possibility remains that its sorting or turnover is misregulated, resulting in amplified signaling. Second, the Toll adaptor MyD88 binds PIP_2, and is mislocalized from the plasma membrane to intracellular compartments in *docrl* mutants (**Fig 6C**). Third, and perhaps most intriguing, our data suggest that hemocyte-autonomous redistribution and increased secretion of the Toll ligand Spz could contribute to aberrant pathway activation and subsequent immune response. We found *docrl* mutant hemocytes exhibited increased levels of both intracellular and secreted Spz. Strikingly, we found that Rab11-mediated rescue of *docrl* innate immune activation correlated with increased intracellular retention and thus diminished secretion of Spz, strongly suggesting that Spz release is a primary driver of innate immune activation (**Fig 6D-G**). Taken together, our data suggest that Spz is normally degraded by an endolysosomal pathway. In *docrl* mutants, this pathway is defective (**Fig 4A, D**), leading to accumulation of Spz and its release into the hemolymph, promoting immune activation. Aberrant fusion of Spz-containing compartments with the plasma membrane may arise directly from altered endosomal membrane composition in *docrl* mutants: Previous studies have shown that PIP2-rich membranes are favored for plasma membrane fusion [55], and the membrane composition of late endosomes correlates with plasma membrane or lysosome fusion [56, 57]. Finally, activation of Rab11 may rescue aberrant Spz release by redirecting it from secretion into hemolymph to a canonical recycling pathway. In the future, it will be interesting to determine whether and how similar changes in Spz trafficking may participate in normal immune responses.

Relevance to Lowe Syndrome

Here, we showed that *docrl* is required specifically in cells of the innate immune

system to suppress spurious activity. One interesting hypothesis is that innate immune phenotypes might underlie epilepsy and cystic brain lesions in Lowe Syndrome patients [58]. There is strong evidence for a link between inflammation, innate immunity, and epilepsy [59]. Most strikingly, a recent report implicates that early immune challenge by LPS in mice promotes an astrocytic TLR4-MyD88 signaling pathway that enhances excitatory synaptogenesis and subsequent seizure susceptibility [60]. Several studies also suggest a direct link between OCRL, neuroinflammation, and seizure. Zebrafish *ocrl* mutants feature cystic lesions in the brain that are enriched in glia, and exhibit seizure susceptibility [14]. Further, pilocarpine seizure induction in mice led to decreased accumulation of OCRL in hippocampal astrocytes [61]. Though it remains unclear in this case whether these changes are pathological or compensatory, it will be important to investigate the link between OCRL and seizure in these mammalian systems. Together, these data raise the possibility that loss of OCRL causes seizures in humans due to immune activation in the brain, by mechanisms similar to those we have uncovered in *Drosophila*. Thus, our finding that dOCRL acts specifically in immune cells to restrain innate immune activation provides a novel line of inquiry into the pathogenesis of the symptoms in Lowe Syndrome patients.

EXPERIMENTAL PROCEDURES

Statistical methods

All graphs show mean ± SEM. Statistical significance was calculated with Prism software (GraphPad, La Jolla, CA) as follows for specific datasets: We used one-way ANOVA followed by pairwise Tukey's test (**Figs 1A**, **1F**, **3E**, **4B**, **4D** (intensity), **5A**, **5D**, **6F**, **S4C**, **S5**), or Kruskal-Wallis test with post-hoc Dunn's test (**Figs 1B**, **1F**, **2E**, **2F**, **3B**, **4C**, **5B**, **6A**, **6G**, **S6** (whole cell & nuclear DI)). For comparisons between two groups, we utilized Student's *t* test (**Figs 6C-E**, **S6A** (% nuclear)) or Mann-Whitney U test (**Fig 3D** (PCC), **6B**). Chi squared tests were used to calculate differences from expected distributions of cell types. In all cases $*p < 0.05$, $**p < 0.01$, $***p < 0.001$.

Drosophila strains and methods

Drosophila larvae were cultured using standard media at low density at 25ºC for all experiments, unless noted otherwise. To generate *docrl* mutants, P[EPgy2]EY15890 (732 bp upstream of the *docrl* start codon) was mobilized using a Δ2-3 transposase, in the *mus309* mutant background for $docrl^{\Delta pre}$, $docrl^{\Delta 1}$, $docrl^{\Delta 2}$, and $docrl^{\Delta 3}$ [62]. 600 candidate lines were screened by PCR to identify deletions, which were subsequently sequenced to determine precise molecular coordinates. Line $docrl^{\Delta pre}$ contains a sequence-verified precise excision of the P-element. dOCRL and VPS35 were cloned using Gateway technology (Life Technologies, Inc) into pBI-UASc-gateway-eGFP [63]. Constructs were injected into flies (Genetic Services Inc. Cambridge, MA), using Φc31 recombinase at the Attp40 locus [64].

Additional fly strains used have been previously described (and where noted with BL stock numbers, are available at the Bloomington *Drosophila* Stock Center) as follows. Alleles: *vps26* (BL26623), $snx1^{\Delta 2}$ and $snx3^{\Delta 1}$ [65], $Df(X)^{ED6565}$ (BL9299), $Dup(X)^{DC402}$ [66]. Drivers: He-Gal4 (BL8699, [30]), Lsp2-Gal4 [67], Dot-Gal4 (BL6902, [27]). Endogenously labeled proteins: $dOCRL^{T\text{-}STEP}$ [32] and Rab GTPases [68]. Expression lines: UAS-Spz-GFP [69], UAS-Toll-Venus [70], UAS-GFP-mCherry-Atg8a [41], UAS-Clc-GFP (BL7109, Henry Chang), $UAS\text{-}OCRL^{ptase}$ [35]., UAS-PHPLC-cherry (BL51658, [71]), $UAS\text{-}shi^{TS}$ (BL44222), $UAS\text{-}shi^{K44A}$ (BL5811), UAS-lacZ (BL1777), $UAS\text{-}Rab11^{QL}$ [72], $rab11^{N124I}$ [73]. Remaining UAS-Rab constructs including $YFP\text{-}Rab5^{QL}$ (BL9773), $rab7^{QL}$ (BL9779), $rab7^{SN}$ (BL9778), $rab5^{SN}$ (BL42704), $rab35^{SN}$ (BL9820) were described in [74].

Hemocyte extraction, quantification and immunocytochemistry

Wandering 3rd instar larvae were used for all hemocyte experiments. Hemolymph was extracted from individual larva or groups of 2-5 larvae. Larvae were collected into PBS, quickly washed with 70% ethanol and then rinsed three times in PBS. Hemolymph was collected by tearing the larval cuticle into PBS with 0.01% phenylthiourea. For absolute hemocyte counts (**Fig 1A-B**), hemolymph was loaded onto each side of a disposable hemocytometer (Incyto C-Chip DHC-N01) and allowed to settle for 30 minutes in a moist chamber before quantification of GFP positive cells using a 20x objective on an EVOS FL Cell Imaging System. For relative hemocyte counts (**Fig 1F, 3E, 5A, 5D**) and

immunocytochemistry, hemolymph was extracted into PBS from 2 or more pooled larvae, and placed in each well of a multi-chamber microscope slide (Thermo Scientific Nunc Lab-Tek II 8-chamber slides). Each well, containing an independent collection of hemocytes from pooled larvae, represents a single sample. Hemocytes were allowed to settle for 60 minutes in a moist chamber at room temperature and then fixed for 10 minutes in 4% formaldehyde in PBS, washed in PBS, and then permeabilized, stained with primary and secondary antibodies and washed with PBX (PBS with 0.1% Triton-x-100). Slides were mounted with Mowiol with DABCO. Cells were imaged by either confocal or widefield microscopy, and counted from at least 6 fields of view per sample.

Antibodies

A fragment of dOCRL encoding amino acids 1-179 was cloned into pGEX-6P (GE Healthcare). *E. coli* strain BL21(DE3) expressing this construct was grown to log phase at 37ºC, then induced for 3 h at 37ºC with 0.4 mM IPTG. Cells were lysed in PBS (phosphate-buffered saline, pH 7.4) supplemented with 0.5 mM DTT, 0.5% Triton-X100, 0.5 mg/ml pepstatin, leupeptin and aprotonin and 1 mM PMSF. Lysates were purified on glutathione agarose (GE Healthcare), washed 4 times with 50 ml of PBS with 0.5 mM DTT, and GST was cleaved from dOCRL$^{1-178}$ at 4º overnight with a ~1:50 molar ratio of Precision Protease (GE Healthcare). Supernatant containing the cleaved protein was further purified by gel filtration on a Superose 12 10/30 column equilibrated in PBS with 0.5 mM DTT. Purified protein was flash frozen in liquid nitrogen at a final concentration of 0.3 mg/ml, and sent to Cocalico, Inc. for injection into rabbits. Serum from Rabbit #18 was affinity purified against GST-dOCRL$^{1-178}$, which was expressed as above, purified on a Profinia system (Biorad) with a glutathione affinity column, and eluted with glutathione according to manufacturer's instructions. Glutathione eluates were gel filtered into PBS on a Sephacryl S-200 16/60 column (GE Healthcare), and conjugated to an Aminolink immobilization column (Thermo-Pierce) using the cyanoborohydride method, according to manufacturer's instructions. 2 mL of α-dOCRL serum from Rabbit #18 were incubated for 2 h on the resin, then washed 5 times with 2 mL PBS, and eluted with 0.1 M glycine, pH 2.5. The eluate was then neutralized by adding Tris pH 9.0 to a final concentration of 25 mM, and stored at 4ºC. Additional antibodies used were

anti-L1 and P1 (gift of Istvan Ando) anti-Lamin Dm0 (DSHB ADL67.10), anti-Spz (gift of S. Goto), anti-MyD88 (gift of S. Wasserman), anti-actin (DSHB JLA20), anti-pH3 (Abcam ab5176).

Phagocytosis and endocytosis assays

To measure phagocytosis, hemocytes were extracted and spread on slides for 30 min as described above. Cells were then washed twice with PBS, and incubated for the indicated times with 100 µl PBS containing $6x10^6$ particles Alexa 488-labeled E. coli (Life Technologies). Cells were then washed quickly 5 times with 500 µl PBS before fixing and imaging as above.

Receptor-mediated and bulk endocytosis were measured essentially as previously described [40, 75]. Specifically, hemocytes were extracted and spread for 5 minutes on slides as described for immunocytochemistry, then pulsed for 45 sec with 5ug/mL Cy5-labeled maleylated BSA (see below) in M1 medium (150 mM NaCl, 5 mM KCl, 1 mM CaCl2, 1 mM MgCl2, 20 mM HEPES, pH 6.9; supplemented with BSA (1.5 mg/ml) and D-glucose (2 mg/ml)), and chased with M1 medium at room temperature. Cells were then fixed and imaged as above. Cy5-labeled maleylated BSA (Cy5-mBSA) was prepared as described in [76] and labeled with bis-functional Cy5 according to manufacturer's instructions (GE Healthcare)).

Immunoblots of whole larva and hemolymph extracts

Whole 3rd instar larvae were homogenized in Laemmli sample buffer (20 µl/larvae) and boiled for 1 min. 10 µl (the equivalent of 0.5 larvae) were loaded for immunoblotting. Larval hemolymph was isolated as follows: A ~2mm slit was made in the bottom of a 500uL Eppendorf tube and the cap was removed. The indicated number of larvae were pierced at their posterior end by a pair of forceps and added to the prepared tube on ice. The tube was placed in a 1.7mL Eppendorf tube and spun at 1000xG for 10 sec. 50 µl ice cold PBS with 0.01% phenylthiourea was added to hemolymph and centrifuged at 5000 x g for 5 min. 25 µl solution was reserved as cell free hemolymph, and boiled for 1 min in 25 µl Laemmli sample buffer. Boiled samples were centrifuged at 14,000 x g for 1 min before loading on SDS-PAGE gels and transferring to nitrocellulose. Blots were

labeled with Alexa 680-conjugated secondary antibodies, and detected on a LI-COR Odyssey infrared detection system.

Imaging and image analysis

Confocal imaging was conducted on an Andor Revolution spinning disk system consisting of a Nikon Ni-E upright microscope, equipped with 40x (n.a. 1.3), 60X (n.a. 1.4), and 100X (n.a. 1.45) oil immersion objectives, a Yokogawa CSU-W1 spinning disk head, and an Andor iXon 897U EMCCD camera. Confocal imaging was used to acquire data related to protein subcellular localization and abundance (**Figs 2, 3A-D, 4, 6**). Widefield imaging was conducted on a Ni-E inverted microscope equipped with a Spectra-X LED light engine and a Zyla sCMOS camera, and a 60X (n.a. 1.4) objective. Widefield imaging was used to measure cell relative cell counts and actin accumulation (**Fig 1F, 3E-F, 5**). Images were collected using Nikon Elements AR software.

Fluorescence microscopy image processing and analysis was performed in FIJI (National Institutes of Health, Bethesda, MD). Fluorescence intensity measurements (area, perimeter, mean and integrated intensity) were performed on sum intensity projections. Plasma membrane ratio of MyD88 was calculated as follows: Cell profiles of single Z sections taken at the approximate midpoint of the cell body were thresholded in FIJI, and the resulting cell mask was divided into three circumferential regions of approximately equal area. The mean fluorescence intensity in the outer ring (which captured the plasma membrane signal) was divided by the mean fluorescence intensity in the adjacent ring (which captured a representative section of cytoplasm). Pearson R was calculated using Coloc2 (FIJI) on 3D cell image stacks.

Live imaging

1-3 wandering third instar larvae/genotype were bled directly into 50uL M1 medium supplemented with BSA (1.5mg/ml) and D-glucose (2 mg/ml). Hemocytes were allowed to settle 5 minutes, and then coverslips were affixed to a glass slide by double sided tape, which simultaneously served as a bridge (3M). A single experiment was considered to be the aggregate of all cells imaged of a single genotype during a single imaging session, and all relevant comparisons were made only between groups imaged

on the same day (over the course of ~3 hours) imaged with identical settings.

REFERENCES

1. Lewis RA, Nussbaum RL, Brewer ED. Lowe Syndrome. 1993. Epub 2012/02/23. doi: NBK1480 [bookaccession]. PubMed PMID: 20301653.

2. Mehta ZB, Pietka G, Lowe M. The Cellular and Physiological Functions of the Lowe Syndrome Protein OCRL1. Traffic. 2014;15(5):471-87. Epub 2014/02/07. doi: 10.1111/tra.12160. PubMed PMID: 24499450.

3. Cauvin C, Rosendale M, Gupta-Rossi N, Rocancourt M, Larraufie P, Salomon R, et al. Rab35 GTPase Triggers Switch-like Recruitment of the Lowe Syndrome Lipid Phosphatase OCRL on Newborn Endosomes. Curr Biol. 2016;26(1):120-8. Epub 2016/01/05. doi: S0960-9822(15)01434-7 [pii]

10.1016/j.cub.2015.11.040. PubMed PMID: 26725203.

4. Erdmann KS, Mao Y, McCrea HJ, Zoncu R, Lee S, Paradise S, et al. A role of the Lowe syndrome protein OCRL in early steps of the endocytic pathway. Dev Cell. 2007;13(3):377-90. Epub 2007/09/04. doi: S1534-5807(07)00304-8 [pii]

10.1016/j.devcel.2007.08.004. PubMed PMID: 17765681; PubMed Central PMCID: PMC2025683.

5. Nandez R, Balkin DM, Messa M, Liang L, Paradise S, Czapla H, et al. A role of OCRL in clathrin-coated pit dynamics and uncoating revealed by studies of Lowe syndrome cells. Elife. 2014;3. Epub 2014/08/12. doi: 10.7554/eLife.02975. PubMed PMID: 25107275.

6. Billcliff PG, Noakes CJ, Mehta ZB, Yan G, Mak L, Woscholski R, et al. OCRL1 engages with the F-BAR protein pacsin 2 to promote biogenesis of membrane-trafficking intermediates. Mol Biol Cell. 2016;27(1):90-107. Epub 2015/10/30. doi: mbc.E15-06-0329 [pii]

10.1091/mbc.E15-06-0329. PubMed PMID: 26510499; PubMed Central PMCID: PMC4694765.

7. Choudhury R, Diao A, Zhang F, Eisenberg E, Saint-Pol A, Williams C, et al. Lowe syndrome protein OCRL1 interacts with clathrin and regulates protein trafficking between endosomes and the trans-Golgi network. Mol Biol Cell. 2005;16(8):3467-79. Epub 2005/05/27. doi: E05-02-0120 [pii]

10.1091/mbc.E05-02-0120. PubMed PMID: 15917292; PubMed Central PMCID: PMC1182289.

8. Noakes CJ, Lee G, Lowe M. The PH domain proteins IPIP27A and B link OCRL1 to receptor recycling in the endocytic pathway. Mol Biol Cell. 2011;22(5):606-23. Epub 2011/01/15. doi: mbc.E10-08-0730 [pii]

10.1091/mbc.E10-08-0730. PubMed PMID: 21233288; PubMed Central PMCID: PMC3046058.

9. De Leo MG, Staiano L, Vicinanza M, Luciani A, Carissimo A, Mutarelli M, et al. Autophagosome-lysosome fusion triggers a lysosomal response mediated by TLR9 and controlled by OCRL. Nat Cell Biol. 2016. Epub 2016/07/12. doi: ncb3386 [pii]

10.1038/ncb3386. PubMed PMID: 27398910.

10. Dambournet D, Machicoane M, Chesneau L, Sachse M, Rocancourt M, El Marjou A, et al. Rab35 GTPase and OCRL phosphatase remodel lipids and F-actin for successful cytokinesis. Nat Cell Biol. 2011;13(8):981-8. Epub 2011/06/28. doi: ncb2279 [pii]

10.1038/ncb2279. PubMed PMID: 21706022.

11. Faucherre A, Desbois P, Nagano F, Satre V, Lunardi J, Gacon G, et al. Lowe syndrome protein Ocrl1 is translocated to membrane ruffles upon Rac GTPase activation: a new perspective on Lowe syndrome pathophysiology. Hum Mol Genet. 2005;14(11):1441-8. Epub 2005/04/15. doi: ddi153 [pii]

10.1093/hmg/ddi153. PubMed PMID: 15829501.

12. Luo N, Kumar A, Conwell M, Weinreb RN, Anderson R, Sun Y. Compensatory Role of Inositol 5-Phosphatase INPP5B to OCRL in Primary Cilia Formation in Oculocerebrorenal Syndrome of Lowe. PLoS One. 2013;8(6):e66727. Epub 2013/06/28. doi: 10.1371/journal.pone.0066727

PONE-D-13-11031 [pii]. PubMed PMID: 23805271; PubMed Central PMCID: PMC3689662.

13. Ben El Kadhi K, Roubinet C, Solinet S, Emery G, Carreno S. The inositol 5-phosphatase dOCRL controls PI(4,5)P2 homeostasis and is necessary for cytokinesis. Curr Biol. 2011;21(12):1074-9. Epub 2011/06/11. doi: S0960-9822(11)00557-4 [pii]

10.1016/j.cub.2011.05.030. PubMed PMID: 21658948.

14. Ramirez IB, Pietka G, Jones DR, Divecha N, Alia A, Baraban SC, et al. Impaired neural development in a zebrafish model for Lowe syndrome. Hum Mol Genet. 2012;21(8):1744-59. Epub 2012/01/03. doi: ddr608 [pii]

10.1093/hmg/ddr608. PubMed PMID: 22210625; PubMed Central PMCID: PMC3313792.

15. Bothwell SP, Chan E, Bernardini IM, Kuo YM, Gahl WA, Nussbaum RL. Mouse model for Lowe syndrome/Dent Disease 2 renal tubulopathy. J Am Soc Nephrol. 2011;22(3):443-8. Epub 2010/12/25. doi: ASN.2010050565 [pii]

10.1681/ASN.2010050565. PubMed PMID: 21183592; PubMed Central PMCID: PMC3060438.

16. Shilo BZ, Schejter ED. Regulation of developmental intercellular signalling by intracellular trafficking. EMBO J. 2011;30(17):3516-26. Epub 2011/09/01. doi: emboj2011269 [pii]

10.1038/emboj.2011.269. PubMed PMID: 21878993; PubMed Central PMCID: PMC3181488.

17. Korolchuk VI, Schutz MM, Gomez-Llorente C, Rocha J, Lansu NR, Collins SM, et al. Drosophila Vps35 function is necessary for normal endocytic trafficking and actin cytoskeleton organisation. J Cell Sci. 2007;120(Pt 24):4367-76. Epub 2007/12/07. doi: 120/24/4367 [pii]

10.1242/jcs.012336. PubMed PMID: 18057029.

18. Shravage BV, Hill JH, Powers CM, Wu L, Baehrecke EH. Atg6 is required for multiple vesicle trafficking pathways and hematopoiesis in Drosophila. Development. 2013;140(6):1321-9. Epub 2013/02/15. doi: dev.089490 [pii]

10.1242/dev.089490. PubMed PMID: 23406899; PubMed Central PMCID: PMC3585664.

19. Jean S, Cox S, Schmidt EJ, Robinson FL, Kiger A. Sbf/MTMR13 coordinates PI(3)P and Rab21 regulation in endocytic control of cellular remodeling. Mol Biol Cell. 2012;23(14):2723-40. Epub 2012/06/01. doi: mbc.E12-05-0375 [pii]

10.1091/mbc.E12-05-0375. PubMed PMID: 22648168; PubMed Central PMCID: PMC3395661.

20. Khadilkar RJ, Rodrigues D, Mote RD, Sinha AR, Kulkarni V, Magadi SS, et al. ARF1-GTP regulates Asrij to provide endocytic control of Drosophila blood cell homeostasis. Proc Natl Acad Sci U S A. 2014;111(13):4898-903. Epub 2014/04/08. doi: 1303559111 [pii]

10.1073/pnas.1303559111. PubMed PMID: 24707047; PubMed Central PMCID: PMC3977295.

21. Zhou B, Yun EY, Ray L, You J, Ip YT, Lin X. Retromer promotes immune quiescence by suppressing Spatzle-Toll pathway in Drosophila. J Cell Physiol. 2014;229(4):512-20. Epub 2013/12/18. doi: 10.1002/jcp.24472. PubMed PMID: 24343480.

22. Matova N, Anderson KV. Drosophila Rel proteins are central regulators of a robust, multi-organ immune network. J Cell Sci. 2010;123(Pt 4):627-33. Epub 2010/02/11. doi: 123/4/627 [pii]

10.1242/jcs.060731. PubMed PMID: 20145002; PubMed Central PMCID: PMC2818199.

23. Minakhina S, Steward R. Melanotic mutants in Drosophila: pathways and phenotypes. Genetics. 2006;174(1):253-63. Epub 2006/07/04. doi: genetics.106.061978 [pii]

10.1534/genetics.106.061978. PubMed PMID: 16816412; PubMed Central PMCID: PMC1569781.

24. Crozatier M, Meister M. Drosophila haematopoiesis. Cell Microbiol. 2007;9(5):1117-26. Epub 2007/03/31. doi: CMI930 [pii]

10.1111/j.1462-5822.2007.00930.x. PubMed PMID: 17394559.

25. Schmid MR, Anderl I, Vesala L, Vanha-aho LM, Deng XJ, Ramet M, et al. Control of Drosophila blood cell activation via Toll signaling in the fat body. PLoS One. 2014;9(8):e102568. Epub 2014/08/08. doi: 10.1371/journal.pone.0102568

PONE-D-14-13634 [pii]. PubMed PMID: 25102059; PubMed Central PMCID: PMC4125153.

26. Soukup SF, Culi J, Gubb D. Uptake of the necrotic serpin in Drosophila melanogaster via the lipophorin receptor-1. PLoS Genet. 2009;5(6):e1000532. Epub 2009/06/27. doi: 10.1371/journal.pgen.1000532. PubMed PMID: 19557185; PubMed Central PMCID: PMC2694266.

27. Kimbrell DA, Hice C, Bolduc C, Kleinhesselink K, Beckingham K. The Dorothy enhancer has Tinman binding sites and drives hopscotch-induced tumor formation. Genesis. 2002;34(1-2):23-8. Epub 2002/09/27. doi: 10.1002/gene.10134. PubMed PMID: 12324942.

28. Honti V, Csordas G, Kurucz E, Markus R, Ando I. The cell-mediated immunity of Drosophila melanogaster: hemocyte lineages, immune compartments, microanatomy and regulation. Dev Comp Immunol. 2014;42(1):47-56. Epub 2013/06/27. doi: S0145-305X(13)00168-7 [pii]

10.1016/j.dci.2013.06.005. PubMed PMID: 23800719.

29. Honti V, Csordas G, Markus R, Kurucz E, Jankovics F, Ando I. Cell lineage tracing reveals the plasticity of the hemocyte lineages and of the hematopoietic compartments in Drosophila melanogaster. Mol Immunol. 2010;47(11-12):1997-2004. Epub 2010/05/21. doi: S0161-5890(10)00156-2 [pii]

10.1016/j.molimm.2010.04.017. PubMed PMID: 20483458.

30. Zettervall CJ, Anderl I, Williams MJ, Palmer R, Kurucz E, Ando I, et al. A directed screen for genes involved in Drosophila blood cell activation. Proc Natl Acad Sci U S A. 2004;101(39):14192-7. Epub 2004/09/24. doi: 10.1073/pnas.0403789101

0403789101 [pii]. PubMed PMID: 15381778; PubMed Central PMCID: PMC521135.

31. Williams MJ, Wiklund ML, Wikman S, Hultmark D. Rac1 signalling in the Drosophila larval cellular immune response. J Cell Sci. 2006;119(Pt 10):2015-24. Epub 2006/04/20. doi: jcs.02920 [pii]

10.1242/jcs.02920. PubMed PMID: 16621891.

32. Koles K, Yeh AR, Rodal AA. Tissue-specific tagging of endogenous loci in Drosophila melanogaster. Biol Open. 2015;5(1):83-9. Epub 2015/12/25. doi: bio.016089 [pii]

10.1242/bio.016089. PubMed PMID: 26700726; PubMed Central PMCID: PMC4728311.

33. Hammond GR, Balla T. Polyphosphoinositide binding domains: Key to inositol lipid biology. Biochim Biophys Acta. 2015;1851(6):746-58. Epub 2015/03/04. doi: S1388-1981(15)00061-X [pii]

10.1016/j.bbalip.2015.02.013. PubMed PMID: 25732852; PubMed Central PMCID: PMC4380703.

34. Lin T, Orrison BM, Leahey AM, Suchy SF, Bernard DJ, Lewis RA, et al. Spectrum of mutations in the OCRL1 gene in the Lowe oculocerebrorenal syndrome. Am J Hum Genet. 1997;60(6):1384-8. Epub 1997/06/01. doi: S0002-9297(07)64230-X [pii]

10.1086/515471. PubMed PMID: 9199559; PubMed Central PMCID: PMC1716142.

35. Guglielmi G, Barry JD, Huber W, De Renzis S. An Optogenetic Method to Modulate Cell Contractility during Tissue Morphogenesis. Dev Cell. 2015;35(5):646-60. Epub 2016/01/19. doi: S1534-5807(15)00685-1 [pii]

10.1016/j.devcel.2015.10.020. PubMed PMID: 26777292; PubMed Central PMCID: PMC4683098.

36. Manaka J, Kuraishi T, Shiratsuchi A, Nakai Y, Higashida H, Henson P, et al. Draper-mediated and phosphatidylserine-independent phagocytosis of apoptotic cells by Drosophila hemocytes/macrophages. J Biol Chem. 2004;279(46):48466-76. Epub 2004/09/03. doi: 10.1074/jbc.M408597200

M408597200 [pii]. PubMed PMID: 15342648.

37. Kurucz E, Markus R, Zsamboki J, Folkl-Medzihradszky K, Darula Z, Vilmos P, et al. Nimrod, a putative phagocytosis receptor with EGF repeats in Drosophila plasmatocytes. Curr Biol. 2007;17(7):649-54. Epub 2007/03/17. doi: S0960-9822(07)01018-4 [pii]

10.1016/j.cub.2007.02.041. PubMed PMID: 17363253.

38. Abrams JM, Lux A, Steller H, Krieger M. Macrophages in Drosophila embryos and L2 cells exhibit scavenger receptor-mediated endocytosis. Proc Natl Acad Sci U S A. 1992;89(21):10375-9. Epub 1992/11/01. PubMed PMID: 1438223; PubMed Central PMCID: PMC50341.

39. Franc NC, Heitzler P, Ezekowitz RA, White K. Requirement for croquemort in phagocytosis of apoptotic cells in Drosophila. Science. 1999;284(5422):1991-4. Epub 1999/06/18. doi: 7588 [pii]. PubMed PMID: 10373118.

40. Guha A, Sriram V, Krishnan KS, Mayor S. Shibire mutations reveal distinct dynamin-independent and -dependent endocytic pathways in primary cultures of Drosophila hemocytes. J Cell Sci. 2003;116(Pt 16):3373-86. Epub 2003/07/15. doi: 10.1242/jcs.00637

116/16/3373 [pii]. PubMed PMID: 12857788.

41. Nezis IP, Shravage BV, Sagona AP, Lamark T, Bjorkoy G, Johansen T, et al. Autophagic degradation of dBruce controls DNA fragmentation in nurse cells during late Drosophila melanogaster oogenesis. J Cell Biol. 2010;190(4):523-31. Epub 2010/08/18. doi: jcb.201002035 [pii]

10.1083/jcb.201002035. PubMed PMID: 20713604; PubMed Central PMCID: PMC2928014.

42. van Weering JR, Cullen PJ. Membrane-associated cargo recycling by tubule-based endosomal sorting. Semin Cell Dev Biol. 2014;31:40-7. Epub 2014/03/20. doi: S1084-9521(14)00043-3 [pii]

10.1016/j.semcdb.2014.03.015. PubMed PMID: 24641888.

43. Lemaitre B, Meister M, Govind S, Georgel P, Steward R, Reichhart JM, et al. Functional analysis and regulation of nuclear import of dorsal during the immune response in Drosophila. EMBO J. 1995;14(3):536-45. Epub 1995/02/01. PubMed PMID: 7859742; PubMed Central PMCID: PMC398111.

44. Qiu P, Pan PC, Govind S. A role for the Drosophila Toll/Cactus pathway in larval hematopoiesis. Development. 1998;125(10):1909-20. Epub 1998/06/18. PubMed PMID: 9550723.

45. Marek LR, Kagan JC. Phosphoinositide binding by the Toll adaptor dMyD88 controls antibacterial responses in Drosophila. Immunity. 2012;36(4):612-22. Epub 2012/04/03. doi: S1074-7613(12)00097-0 [pii]

10.1016/j.immuni.2012.01.019. PubMed PMID: 22464168; PubMed Central PMCID: PMC3354765.

46. Shia AK, Glittenberg M, Thompson G, Weber AN, Reichhart JM, Ligoxygakis P. Toll-dependent antimicrobial responses in Drosophila larval fat body require Spatzle secreted by haemocytes. J Cell Sci. 2009;122(Pt 24):4505-15. Epub 2009/11/26. doi: jcs.049155 [pii]

10.1242/jcs.049155. PubMed PMID: 19934223; PubMed Central PMCID: PMC2787462.

47. Oltrabella F, Pietka G, Ramirez IB, Mironov A, Starborg T, Drummond IA, et al. The Lowe syndrome protein OCRL1 is required for endocytosis in the zebrafish pronephric tubule. PLoS Genet. 2015;11(4):e1005058. Epub 2015/04/04. doi: 10.1371/journal.pgen.1005058

PGENETICS-D-14-02253 [pii]. PubMed PMID: 25838181; PubMed Central PMCID: PMC4383555.

48. Vicinanza M, Di Campli A, Polishchuk E, Santoro M, Di Tullio G, Godi A, et al. OCRL controls trafficking through early endosomes via PtdIns4,5P(2)-dependent regulation of endosomal actin. EMBO J. 2011;30(24):4970-85. Epub 2011/10/06. doi: emboj2011354 [pii]

10.1038/emboj.2011.354. PubMed PMID: 21971085; PubMed Central PMCID: PMC3242071.

49. Huang HR, Chen ZJ, Kunes S, Chang GD, Maniatis T. Endocytic pathway is required for Drosophila Toll innate immune signaling. Proc Natl Acad Sci U S A. 2010;107(18):8322-7. Epub 2010/04/21. doi: 1004031107 [pii]

10.1073/pnas.1004031107. PubMed PMID: 20404143; PubMed Central PMCID: PMC2889516.

50. Yang H, Kronhamn J, Ekstrom JO, Korkut GG, Hultmark D. JAK/STAT signaling in Drosophila muscles controls the cellular immune response against parasitoid infection. EMBO Rep. 2015;16(12):1664-72. Epub 2015/09/29. doi: embr.201540277 [pii]

10.15252/embr.201540277. PubMed PMID: 26412855; PubMed Central PMCID: PMC4687419.

51. Davis MM, Engstrom Y. Immune response in the barrier epithelia: lessons from the fruit fly Drosophila melanogaster. J Innate Immun. 2012;4(3):273-83. Epub 2012/01/13. doi: 000332947 [pii]

10.1159/000332947. PubMed PMID: 22237424.

52. Zang Y, Wan M, Liu M, Ke H, Ma S, Liu LP, et al. Plasma membrane overgrowth causes fibrotic collagen accumulation and immune activation in Drosophila adipocytes. Elife. 2015;4:e07187. Epub 2015/06/20. doi: 10.7554/eLife.07187. PubMed PMID: 26090908; PubMed Central PMCID: PMC4490375.

53. Brubaker SW, Bonham KS, Zanoni I, Kagan JC. Innate immune pattern recognition: a cell biological perspective. Annu Rev Immunol. 2015;33:257-90. Epub 2015/01/13. doi: 10.1146/annurev-immunol-032414-112240. PubMed PMID: 25581309.

54. Maminska A, Bartosik A, Banach-Orlowska M, Pilecka I, Jastrzebski K, Zdzalik-Bielecka D, et al. ESCRT proteins restrict constitutive NF-kappaB signaling by trafficking cytokine receptors. Sci Signal. 2016;9(411):ra8. Epub 2016/01/21. doi: 9/411/ra8 [pii]

10.1126/scisignal.aad0848. PubMed PMID: 26787452.

55. Ketel K, Krauss M, Nicot AS, Puchkov D, Wieffer M, Muller R, et al. A phosphoinositide conversion mechanism for exit from endosomes. Nature. 2016;529(7586):408-12. Epub 2016/01/14. doi: nature16516 [pii]

10.1038/nature16516. PubMed PMID: 26760201.

56. Mobius W, Ohno-Iwashita Y, van Donselaar EG, Oorschot VM, Shimada Y, Fujimoto T, et al. Immunoelectron microscopic localization of cholesterol using biotinylated and non-cytolytic perfringolysin O. J Histochem Cytochem. 2002;50(1):43-55. Epub 2001/12/19. doi: 10.1177/002215540205000105. PubMed PMID: 11748293.

57. Wubbolts R, Leckie RS, Veenhuizen PT, Schwarzmann G, Mobius W, Hoernschemeyer J, et al. Proteomic and biochemical analyses of human B cell-derived exosomes. Potential implications for their function and multivesicular body formation. J Biol Chem. 2003;278(13):10963-72. Epub 2003/01/10. doi: 10.1074/jbc.M207550200

M207550200 [pii]. PubMed PMID: 12519789.

58. Allmendinger AM, Desai NS, Burke AT, Viswanadhan N, Prabhu S. Neuroimaging and renal ultrasound manifestations of Oculocerebrorenal syndrome of Lowe. J Radiol Case Rep. 2014;8(10):1-7. Epub 2014/11/27. doi: 10.3941/jrcr.v8i10.1740

jrcr-8-10-1 [pii]. PubMed PMID: 25426219; PubMed Central PMCID: PMC4242147.

59. Legido A, Katsetos CD. Experimental studies in epilepsy: immunologic and inflammatory mechanisms. Semin Pediatr Neurol. 2014;21(3):197-206. Epub 2014/12/17. doi: S1071-9091(14)00076-X [pii]

10.1016/j.spen.2014.10.001. PubMed PMID: 25510941.

60. Shen Y, Qin H, Chen J, Mou L, He Y, Yan Y, et al. Postnatal activation of TLR4 in astrocytes promotes excitatory synaptogenesis in hippocampal neurons. J Cell Biol. 2016;215(5):719-34. Epub 2016/12/07. doi: jcb.201605046 [pii]

10.1083/jcb.201605046. PubMed PMID: 27920126; PubMed Central PMCID: PMC5147000.

61. Clasadonte J, Morel L, Barrios-Camacho CM, Chiang MS, Zhang J, Iyer L, et al. Molecular analysis of acute and chronic reactive astrocytes in the pilocarpine model of temporal lobe epilepsy. Neurobiol Dis. 2016;91:315-25. Epub 2016/04/10. doi: S0969-9961(16)30070-5 [pii]

10.1016/j.nbd.2016.03.024. PubMed PMID: 27060558.

62. Witsell A, Kane DP, Rubin S, McVey M. Removal of the bloom syndrome DNA helicase extends the utility of imprecise transposon excision for making null mutations in Drosophila. Genetics. 2009;183(3):1187-93. Epub 2009/08/19. doi: genetics.109.108472 [pii]

10.1534/genetics.109.108472. PubMed PMID: 19687136; PubMed Central PMCID: PMC2778970.

63. Wang JW, Brent JR, Tomlinson A, Shneider NA, McCabe BD. The ALS-associated proteins FUS and TDP-43 function together to affect Drosophila locomotion and life span. J Clin Invest. 2011;121(10):4118-26. Epub 2011/09/02. doi: 57883 [pii]

10.1172/JCI57883. PubMed PMID: 21881207; PubMed Central PMCID: PMC3195475.

64. Ni JQ, Markstein M, Binari R, Pfeiffer B, Liu LP, Villalta C, et al. Vector and parameters for targeted transgenic RNA interference in Drosophila melanogaster. Nat Methods. 2008;5(1):49-51. Epub 2007/12/18. doi: nmeth1146 [pii]

10.1038/nmeth1146. PubMed PMID: 18084299; PubMed Central PMCID: PMC2290002.

65. Zhang P, Wu Y, Belenkaya TY, Lin X. SNX3 controls Wingless/Wnt secretion through regulating retromer-dependent recycling of Wntless. Cell Res. 2011;21(12):1677-90. Epub 2011/11/02. doi: cr2011167 [pii]

10.1038/cr.2011.167. PubMed PMID: 22041890; PubMed Central PMCID: PMC3357989.

66. Venken KJ, Popodi E, Holtzman SL, Schulze KL, Park S, Carlson JW, et al. A molecularly defined duplication set for the X chromosome of Drosophila melanogaster. Genetics. 2010;186(4):1111-25. Epub 2010/09/30. doi: genetics.110.121285 [pii]

10.1534/genetics.110.121285. PubMed PMID: 20876565; PubMed Central PMCID: PMC2998297.

67. Lazareva AA, Roman G, Mattox W, Hardin PE, Dauwalder B. A role for the adult fat body in Drosophila male courtship behavior. PLoS Genet. 2007;3(1):e16. Epub 2007/01/30. doi: 06-PLGE-RA-0274R2 [pii]

10.1371/journal.pgen.0030016. PubMed PMID: 17257054; PubMed Central PMCID: PMC1781494.

68. Dunst S, Kazimiers T, von Zadow F, Jambor H, Sagner A, Brankatschk B, et al. Endogenously tagged rab proteins: a resource to study membrane trafficking in Drosophila. Dev Cell. 2015;33(3):351-65. Epub 2015/05/06. doi: S1534-5807(15)00218-X [pii]

10.1016/j.devcel.2015.03.022. PubMed PMID: 25942626.

69. Stein D, Charatsi I, Cho YS, Zhang Z, Nguyen J, DeLotto R, et al. Localization and activation of the Drosophila protease easter require the ER-resident saposin-like protein seele. Curr Biol. 2010;20(21):1953-8. Epub 2010/10/26. doi: S0960-9822(10)01226-1 [pii]

10.1016/j.cub.2010.09.069. PubMed PMID: 20970335.

70. Mavrakis M, Rikhy R, Lippincott-Schwartz J. Plasma membrane polarity and compartmentalization are established before cellularization in the fly embryo. Dev Cell. 2009;16(1):93-104. Epub 2009/01/22. doi: S1534-5807(08)00477-2 [pii]

10.1016/j.devcel.2008.11.003. PubMed PMID: 19154721; PubMed Central PMCID: PMC2684963.

71. Khuong TM, Habets RL, Slabbaert JR, Verstreken P. WASP is activated by phosphatidylinositol-4,5-bisphosphate to restrict synapse growth in a pathway parallel to bone morphogenetic protein signaling. Proc Natl Acad Sci U S A. 2010;107(40):17379-84. Epub 2010/09/17. doi: 1001794107 [pii]

10.1073/pnas.1001794107. PubMed PMID: 20844206; PubMed Central PMCID: PMC2951409.

72. Emery G, Hutterer A, Berdnik D, Mayer B, Wirtz-Peitz F, Gaitan MG, et al. Asymmetric Rab 11 endosomes regulate delta recycling and specify cell fate in the Drosophila nervous system. Cell. 2005;122(5):763-73. Epub 2005/09/03. doi: S0092-8674(05)00821-4 [pii]

10.1016/j.cell.2005.08.017. PubMed PMID: 16137758.

73. Satoh AK, O'Tousa JE, Ozaki K, Ready DF. Rab11 mediates post-Golgi trafficking of rhodopsin to the photosensitive apical membrane of Drosophila photoreceptors. Development. 2005;132(7):1487-97. Epub 2005/02/25. doi: dev.01704 [pii]

10.1242/dev.01704. PubMed PMID: 15728675.

74. Zhang J, Schulze KL, Hiesinger PR, Suyama K, Wang S, Fish M, et al. Thirty-one flavors of Drosophila rab proteins. Genetics. 2007;176(2):1307-22. Epub 2007/04/06. doi: genetics.106.066761 [pii]

10.1534/genetics.106.066761. PubMed PMID: 17409086; PubMed Central PMCID: PMC1894592.

75. Gupta GD, Swetha MG, Kumari S, Lakshminarayan R, Dey G, Mayor S. Analysis of endocytic pathways in Drosophila cells reveals a conserved role for GBF1 in internalization via GEECs. PLoS One. 2009;4(8):e6768. Epub 2009/08/27. doi: 10.1371/journal.pone.0006768. PubMed PMID: 19707569; PubMed Central PMCID: PMC2728541.

76. Haberland ME, Fogelman AM. Scavenger receptor-mediated recognition of maleyl bovine plasma albumin and the demaleylated protein in human monocyte macrophages. Proc Natl Acad Sci U S A. 1985;82(9):2693-7. Epub 1985/05/01. PubMed PMID: 3857610; PubMed Central PMCID: PMC397631.

FIGURE LEGENDS

Figure 1. dOCRL is required in hemocytes to restrict hemocyte abundance. (A-B) Absolute quantification of hemocytes in hemolymph extracted from wandering third instar larvae. (A) *docrl* mutants exhibit increased circulating hemocytes. (B) Re-expression of dOCRL in hemocytes is sufficient to suppress hemocyte number. (C) *docrl* mutant larvae exhibit melanotic masses, which are rescued by *docrl* gene duplication Dup(1;3)DC402). (D) Frequency of visible melanotic masses. (E) Epifluorescence and reflected light images of a $docrl^{\Delta 3}$ larva showing GFP-labeled hemocytes clustered around a melanotic mass (arrow). Scale bar is 500 μm. (right) 2D projection of confocal image of hemocytes surrounding a melanotic mass. Scale bar is 50 μm. (F) Re-expression of dOCRL-EGFP rescue transgene in hemocytes (he-GAL4), but not nephrocytes (dot-GAL4) or fat body (lsp2-GAL4) fully rescues hemocyte number in $docrl^{\Delta 3}$ larvae. Data are presented as mean +/- SEM. Individual values in A,B,F represent independent samples of hemocytes collected from 2-4 larvae. Sample N in panel D represents number of larvae counted. **Associated with Fig S1 and S2.**

Figure 2. Aberrant immune cell differentiation and activation in *docrl* mutants. (A) 2D projection of confocal image of hemocytes stained for the lamellocyte marker L1 (magenta). Scale bar is 20um. (B) Quantification of L1 staining. Greater numbers of $docrl^{\Delta 3}$ hemocytes are L1-positive (left). This defect is partially rescued by re-expression of dOCRL-EGFP in hemocytes (right). (C) Most $docrl^{\Delta 3}$ L1-positive cells do not exhibit

normal lamellocyte morphology. (D) *docrl*$^{\Delta 3}$ hemocytes exhibit greater F-actin assembly (phalloidin, green) and a spikier morphology than control cells. (E-F) Quantification of F-actin intensity (E) and 'spikiness' (F). Both phenotypes are rescued by hemocyte-autonomous re-expression of dOCRL-EGFP. Data are presented as mean +/- SEM. Sample N in panels B,C represent counted larvae. Data points in E,F represent individual cells.

Figure 3. OCRL regulates PIP2 homeostasis in diverse endosomal compartments. (A) Endogenously tagged dOCRL (magenta) co-localizes strongly with Clc-GFP (green), single channel confocal slices shown below in gray. (B) Pearson correlations between endogenously tagged dOCRL and trafficking compartments in live primary hemocytes. dOCRL localizes only moderately with other endosomal compartments. (C-D) *docrl*$^{\Delta 3}$ hemocytes exhibit increased PH-PLC-Cherry marker of PIP_2 (magenta) in live primary hemocytes in all membrane compartments examined (green) (E) The phosphatase activity of dOCRL is necessary but not sufficient to restrict hemocyte number. (F) Expression of phosphatase alone moderately rescues actin accumulation (phalloidin staining, gray), though actin accumulation at ruffles (arrowhead) and intracellular puncta (arrows) are still observed. Scale bars in A,C,F are 10 μm. Data are presented as mean +/- SEM. Individual values in B,D,F represent single cells. Values in panel E represent independent samples from 2-4 pooled larvae. **Associated with Fig S3.**

Figure 4. Aberrant endosomal compartment structure and function in *docrl* mutants. (A) Loss of *docrl* disrupts the structure of multiple endosomal compartments, including fragmentation and perinuclear accumulation of Clc and Rab5, and expansion of Rab7. Images show single confocal slices. (B) Rab7 levels are increased ~3 fold, while Clc and Rab11 levels are slightly increased. (C) *docrl* mutant hemocytes exhibit defective scavenger receptor mediated endocytosis of mBSA (magenta), panels shown with same brightness and contrast. (D) *docrl* mutants exhibit defective autophagy, marked by GFP-mCherry-Atg8a (GC::Atg8A). Quantification shows Pearson's Correlation Coefficient per cell +/- s.e.m. for GFP and mCherry (left) and mean fluorescence +/- s.e.m. for each fluorophore/cell (right). Scale bars in A,C,D are 10 μm.

Data are presented as mean +/- SEM. Individual values in B,C,D represent single cells. **Associated with Fig S4.**

Figure 5. Endosomal sorting defects underlie hemocyte activation in *docrl* mutants. (A) Relative hemocyte number in larvae with hemocyte-specific manipulation of the indicated Rab GTPases. Inhibiting the internalization step of endocytosis has no effect on hemocyte number, while manipulation of endosomal sorting recapitulates the *docrl* mutant phenotype. Statistical significance noted reflects pairwise tests with wild type control. (B) The phosphatase activity of dOCRL is sufficient to rescue scavenger receptor endocytosis of mBSA. (C) Core retromer and SNX-BAR mutants exhibit melanotic masses. Frequency of visible melanotic masses in wandering third instar larvae. n indicates number of larvae examined. Control is identical to **Fig 1D**. (D) Manipulation of endosomal sorting via Rab11 and Rab7 rescue *docrl*-induced hemocyte overabundance. Data sets were each normalized and statistical significance noted relative to *docrl* mutant controls taken at the same time. Data are presented as mean +/- SEM. Individual values in A,D are independent samples pooled from 2-4 larvae. Each data point in panel B represents a single cell. Sample N in panel C is number of counted larvae. **Associated with Fig S5.**

Figure 6. The Toll pathway is activated in *docrl* mutants. (A) qPCR shows that Toll targets Drs and IM1 are upregulated in *docrl*$^{\Delta 3}$ larvae. (B) He-GAL4-driven Toll-Venus (gray) localizes to intracellular compartments, and exhibits a mild but significant increase in intensity, and slightly broader distribution in *docrl* mutant hemocytes. Images show single confocal Z-plane images of live hemocytes. (C) Localization of the Tl signaling adapter MyD88 in primary hemocytes. MyD88 localizes relocalizes away from the plasma membrane in *docrl* mutant hemocytes. Images show single confocal Z-plane images of fixed hemocytes stained for MyD88. (Right) Schematic and quantification of fraction of plasma membrane MyD88. (D) Spz-GFP accumulation (gray) is mildly, but significantly increased in *docrl*$^{\Delta 3}$ mutant hemocytes. Images show 2D confocal projections of fixed hemocytes. (E) Secreted Spz-GFP is increased in *docrl*$^{\Delta 3}$ hemolymph, measured by western blot of cell-free hemolymph. (F) Hemocyte-specific

expression of Rab11^{CA} causes stronger Spz-GFP (gray) accumulation in *docrl*$^{\Delta 3}$ mutant hemocytes. Images show 2D confocal projections of fixed hemocytes. (G) Hemocyte-specific expression of constitutively active Rab11 rescues the level of Spz-GFP secreted into the hemolymph, by western blot. Statistical significance noted is relative to all other data sets. Scale bars in B-D, F are 10 μm. Data are presented as mean +/- SEM. Individual values in A,C,E are independent samples collected from 3-4 larvae each. N in B-D, F represents single cells. **Associated with Fig S6**.

Figure 7. Model: dOCRL regulates trafficking of Tl pathway components to maintain immune quiescence. (Left) Control cells with a normal endosomal distribution and morphology. MyD88 localizes to plasma membrane and Spz accumulates at low levels in hemocytes and hemolymph. (Center) *docrl* mutant hemocytes exhibit altered endosomal morphology, accumulation, and function, relocalize MyD88 to intracellular puncta, and secrete high levels of Spz. (Right) Rescue with activated Rab11 re-routes Spz and sequesters it in intracellular compartments.

Figure S1 (Associated with Fig 1) Generation of *docrl* mutants. (A) Schematic of the *docrl* locus on the X chromosome. dOCRL domains are color coded across exons, and molecular coordinates of *docrl* excision lines are noted. (B) (Top) Schematic of domain organization of human OCRL1 and dOCRL. Bar indicates N-terminal fragment used to generate α-dOCRL antibodies. The PH domain of OCRL1 is not obviously present in dOCRL. (Bottom) α-dOCRL and α-actin immunoblots of whole third instar larvae. (C) Table of *docrl* mutant viability and complementation tests (n.d.: not determined; xDup indicates Dup(1;3)DC402).

Figure S2 (Associated with Figure 1). *docrl* mutant hemocytes do not exhibit excess mitosis and have a cytokinesis defect. (A) *docrl* mutant hemocytes are not hyper-proliferative. 2D projections of confocal images of hemocytes, fixed and stained with α-lamin Dm0 to label nuclei (red) and α-phospho-histone H3 to label mitotic cells (green). Scale bar is 50 μm. (B-C) *docrl* mutant hemocytes exhibit a cytokinesis defect. (B) Representative multinucleate hemocytes from *docrl* mutants, fixed and stained with

Alexa-488 phalloidin to highlight the cell periphery, and α-lamin Dm0 to stain nuclei. White borders (lower panels) indicate phalloidin-defined cell periphery. Scale bar is 10 μm. (C) Quantification of multinucleate frequency in He-GAL4 UAS-GFP.nls-expressing larvae, and rescue by a genomic dOCRL-containing duplication or by He-GAL4-driven dOCRL-EGFP. Data are presented as mean +/- SEM. Sample N in panel C is number of larvae counted.

Figure S3 (Associated with Figure 3). OCRL localizes to diverse endosomal compartments. (A) All panels are representative single confocal slices from live primary hemocytes that express a TagRFPT-tagged dOCRL expressed from the endogenous *docrl* locus in combination with markers of specific endosomal compartments, as noted. dOCRL localizes most strikingly with Clc-GFP, with strong foci of each colocalizing both at the plasma membrane and in intracellular puncta. dOCRL localizes with YFP-Rab5 and Rab11 more diffusely, and shows a complementary association with Vps35. dOCRL foci are observed also on Rab7 bearing late endosomes. See quantification in **Fig 3B**. (B) All panels are representative single confocal slices from live-imaged primary hemocytes from control $docrl^{\Delta pre}$ and mutant $docrl^{\Delta 3}$ larvae. PIP_2 is marked by expression of UAS-$PH^{PLC\delta}$-cherry in hemocytes under the control of He-GAL4 (magenta). Specific rab compartments (green) are marked by GFP tagged UAS constructs (for Clc and Vps35) or endogenously YFP tagged gene loci (for Rab5, Rab7, and Rab11). $PH^{PLC\delta}$-cherry accumulates in each compartment in $docrl^{\Delta 3}$ hemocytes, relative to controls (see quantification, **Fig 3D**). Scale bars in A,B are 10 μm.

Figure S4 (Associated with Figure 4). *docrl* mutants exhibit disrupted of endosomal compartment structure and function. (A) *docrl* mutant hemocytes exhibit defective endosomal compartment structure. All panels are representative single confocal slices from live primary hemocytes. Vps35 endosomes are fragmented, and Vps35 signal accumulates in a perinuclear region. Rab35 and Rab11 are qualitatively unchanged. (B) *docrl* mutant Rab5 early endosomes are less dynamic than controls. (Left) Single frames from a 2-minute timelapse of a single confocal slice of control and

docrl mutant hemocytes with endogenously labeled GFP-Rab5. (right) Time series color-coded projection of 20-second segments of Rab5 timelapse movies. Multicolor tracks demonstrate greater motility of control Rab5 endosomes relative to *docrl* mutants (white tracks). (C) OCRL mutant hemocytes are competent for phagocytosis. Images show 2D maximum intensity projection of confocal stacks, showing myr-mRFP-expressing hemocytes incubated with Alexa-488 labeled *E. coli*. Inset shows that *E. coli* are intracellular, in 2D maximum intensity projection of XZ view of the cell indicated in the dashed box. (Right) Quantification of mean number of *E. coli* particles, excluding cells with no particles. Data are presented as mean +/- SEM. N represents number of cells measured. Scale bars in A,B,C are 10 μm. Inset scale bar in C is 10 μm.

Figure S5 (associated with Figure 5). Expression of *shi*^{TS} in hemocytes blocks mBSA uptake. (A) Panels represent single confocal slices from primary hemocytes fixed after mBSA uptake, from He>LacZ or He>Shi^{TS} larvae. Scale bar is 10 μm. (B) Quantification of mBSA uptake. Data are presented as mean +/- SEM. N represents number of cells measured.

Figure S6 (Associated with Figure 6). Toll pathway components are misregulated in *docrl* mutant hemocytes. Quantification of the Toll target Dorsal (Dl) in wild type and *docrl* mutant hemocytes. Dl accumulates in both the nucleus and cytoplasm. N represents number of cells measured.

Figure 1

Click here to download Figure Fig1.tiff

Del Signore et al., Figure 1

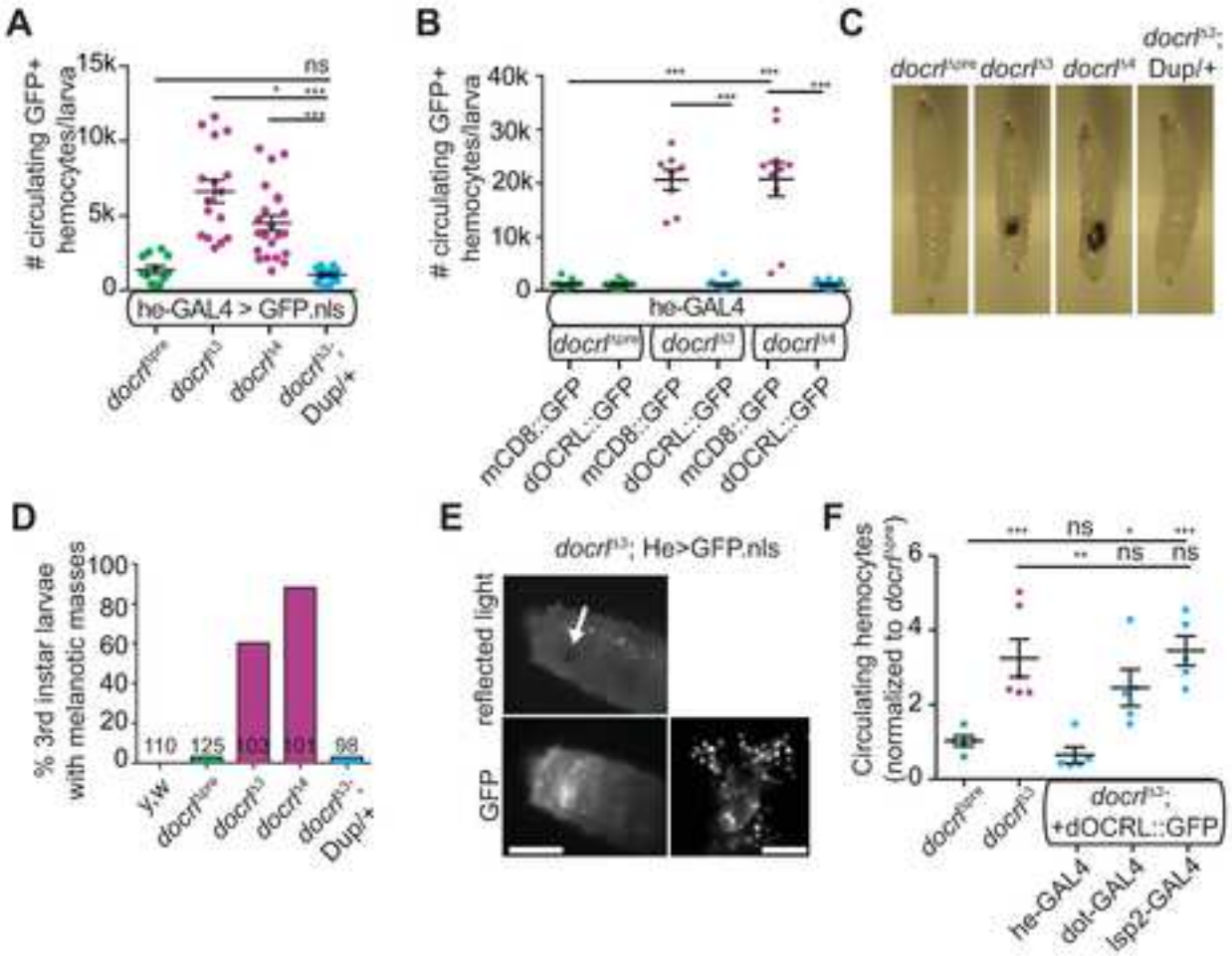

Figure 2

Click here to download Figure Fig2.tiff

Del Signore et al., Figure 2

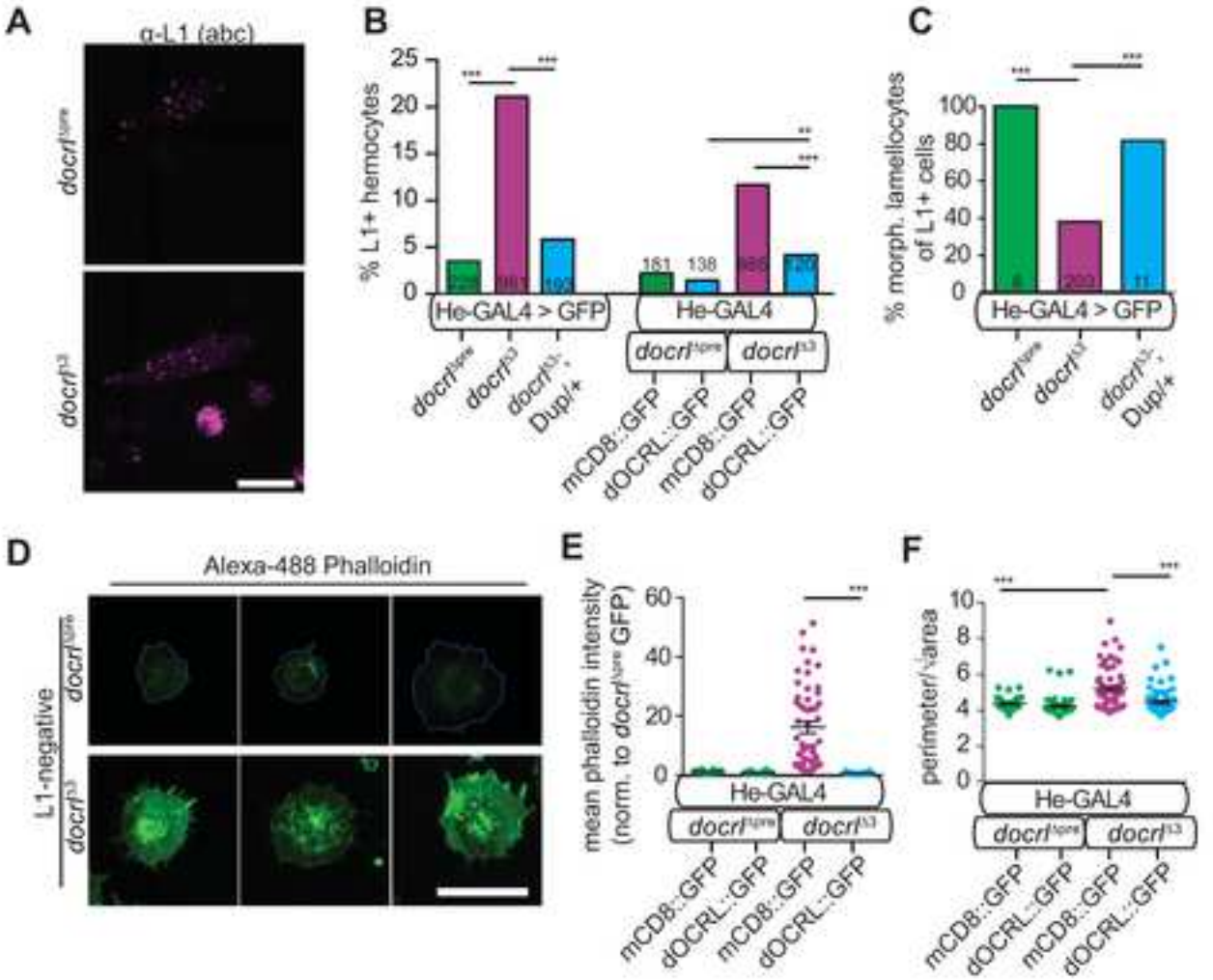

Figure 3

Click here to download Figure Fig3.tiff

Del Signore et al., Figure 3

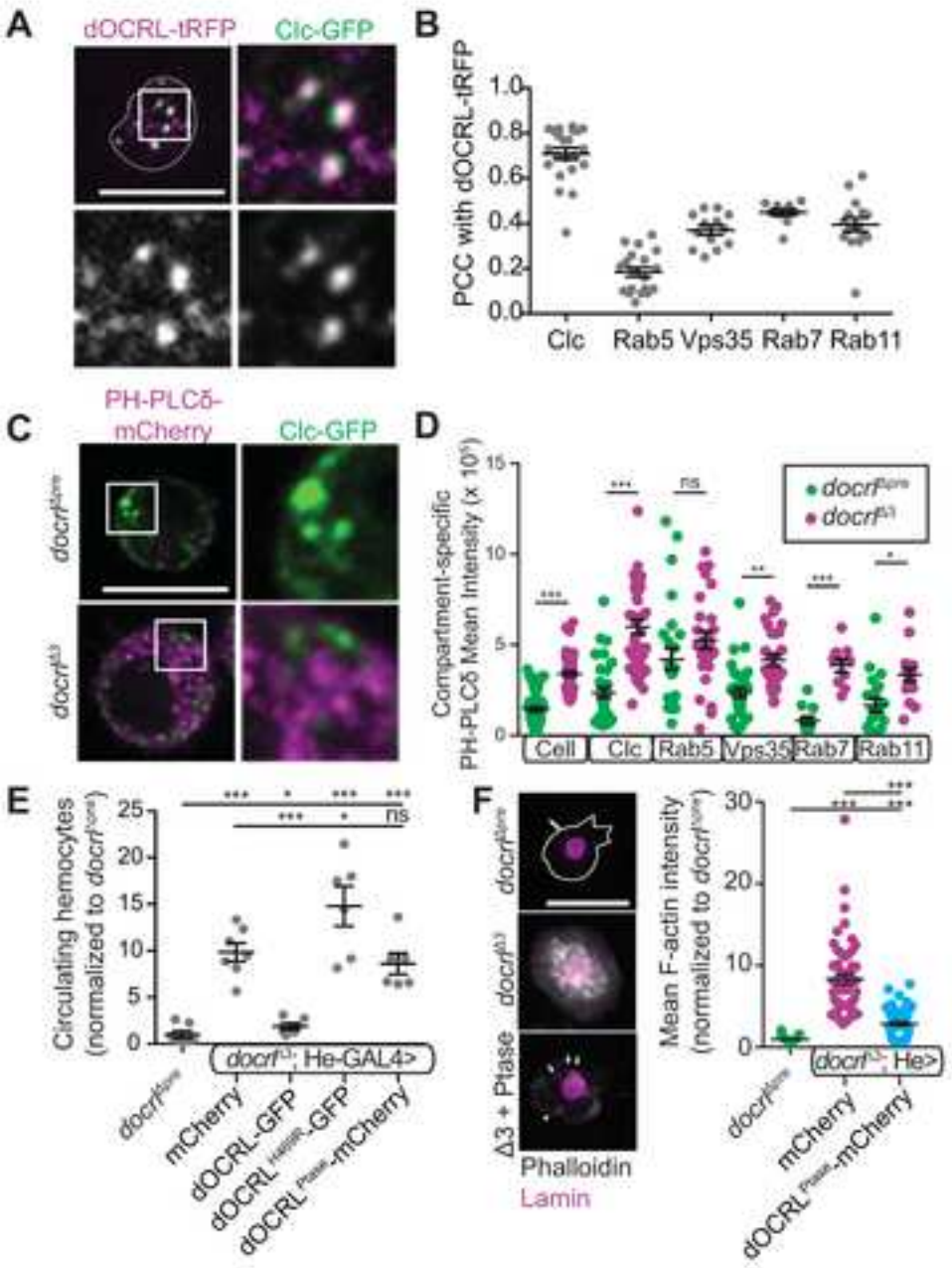

Figure 4

Click here to download Figure Fig4.tiff

Del Signore et al., Figure 4

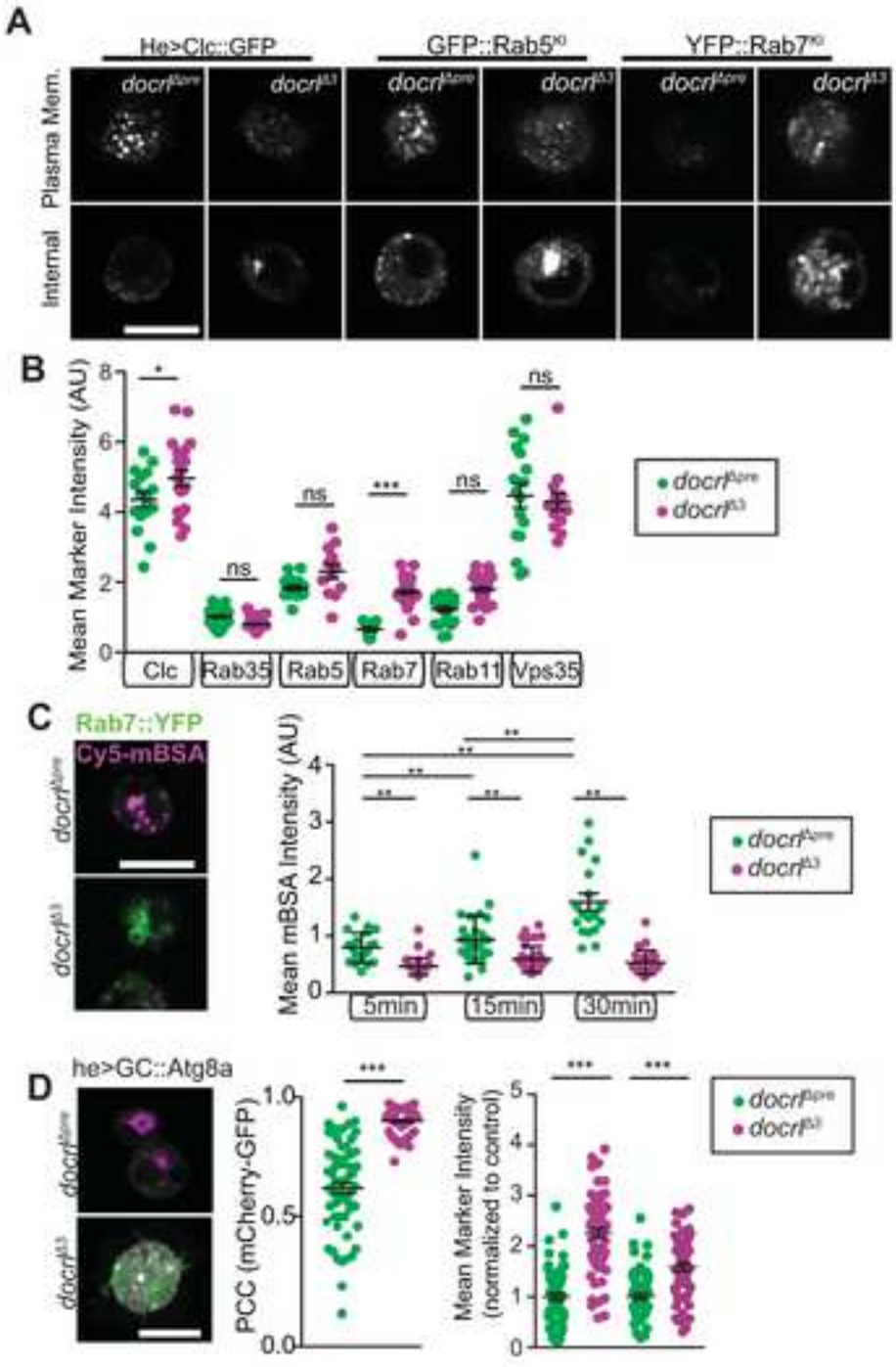

Figure 5

Click here to download Figure Fig5.tiff

Del Signore et al., Figure 5

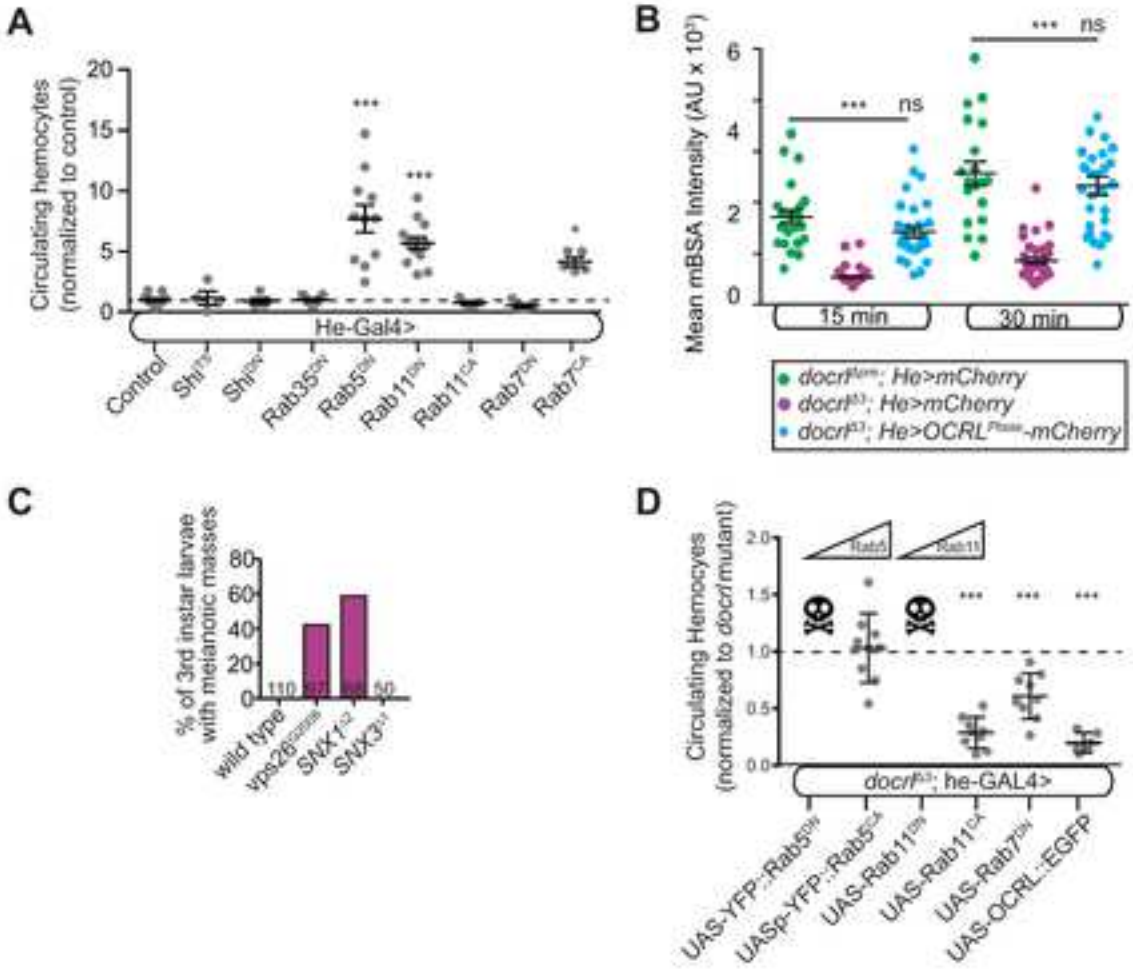

Del Signore et al., Figure 6

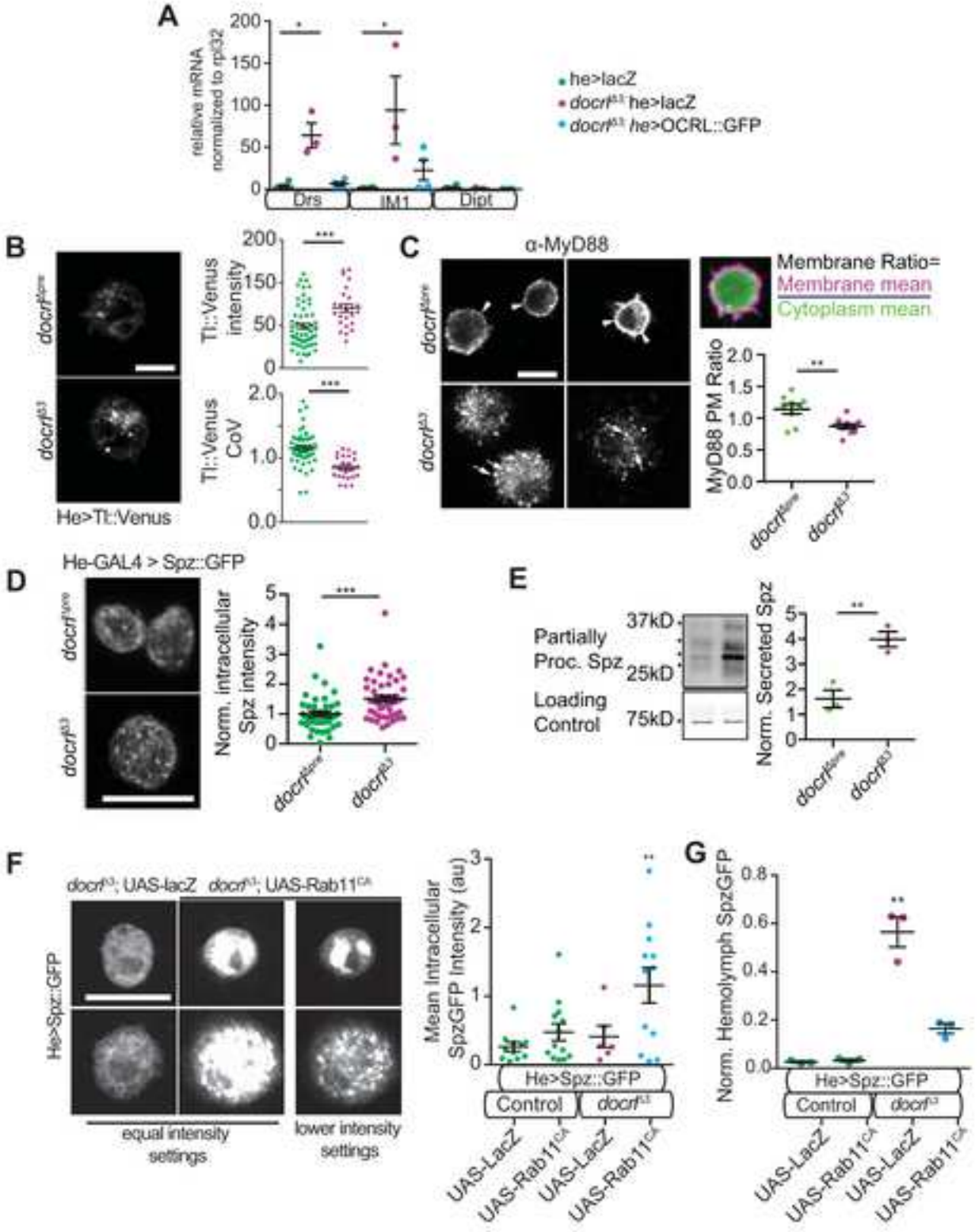

Figure 7

Click here to download Figure Fig7.tiff

Del Signore et al., Figure 7

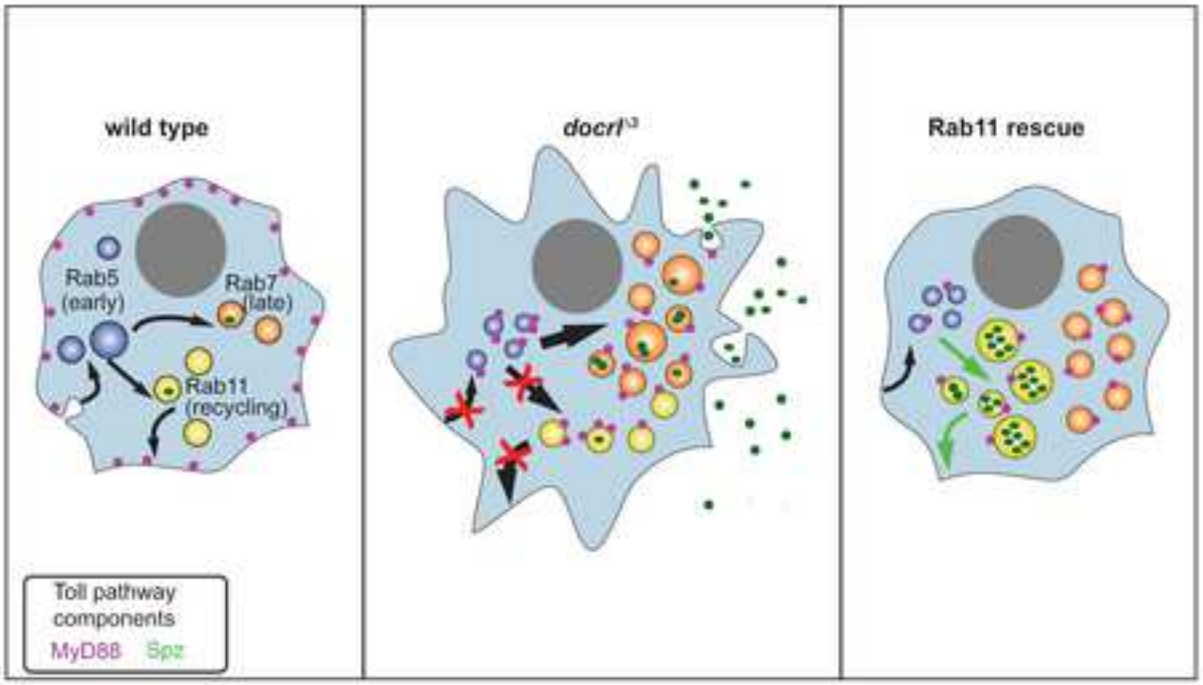

Figure S1

Click here to download Figure FigS1.tiff

Del Signore et al., Figure S1

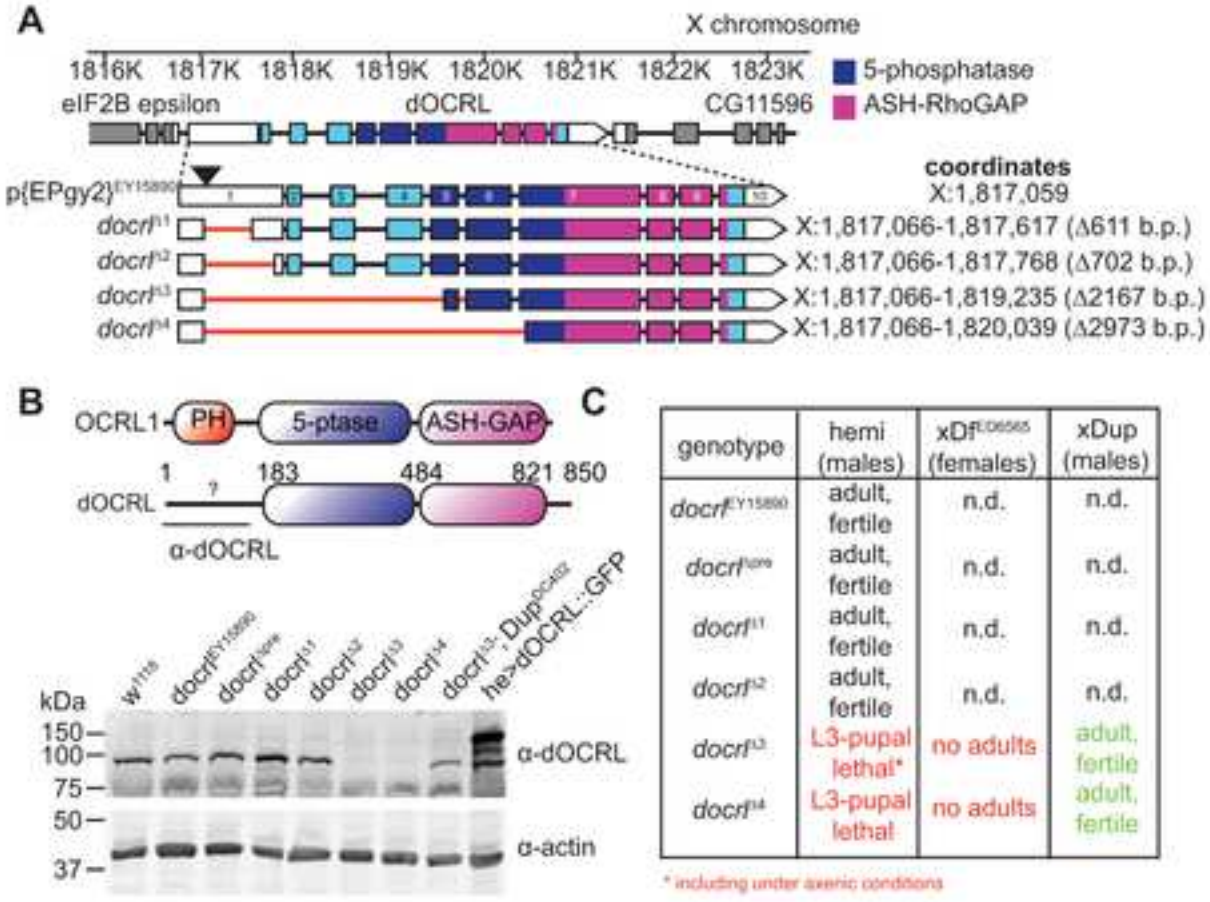

genotype	hemi (males)	xDf^{ED6565} (females)	xDup (males)
docrl^{EY15890}	adult, fertile	n.d.	n.d.
docrl$^{Δ2/9}$	adult, fertile	n.d.	n.d.
docrl^{Δ1}	adult, fertile	n.d.	n.d.
docrl^{Δ2}	adult, fertile	n.d.	n.d.
docrl^{Δ3}	L3-pupal lethal*	no adults	adult, fertile
docrl^{Δ4}	L3-pupal lethal	no adults	adult, fertile

* including under axenic conditions

Figure S2

Click here to download Figure FigS2.tiff

Del Signore et al., Figure S2

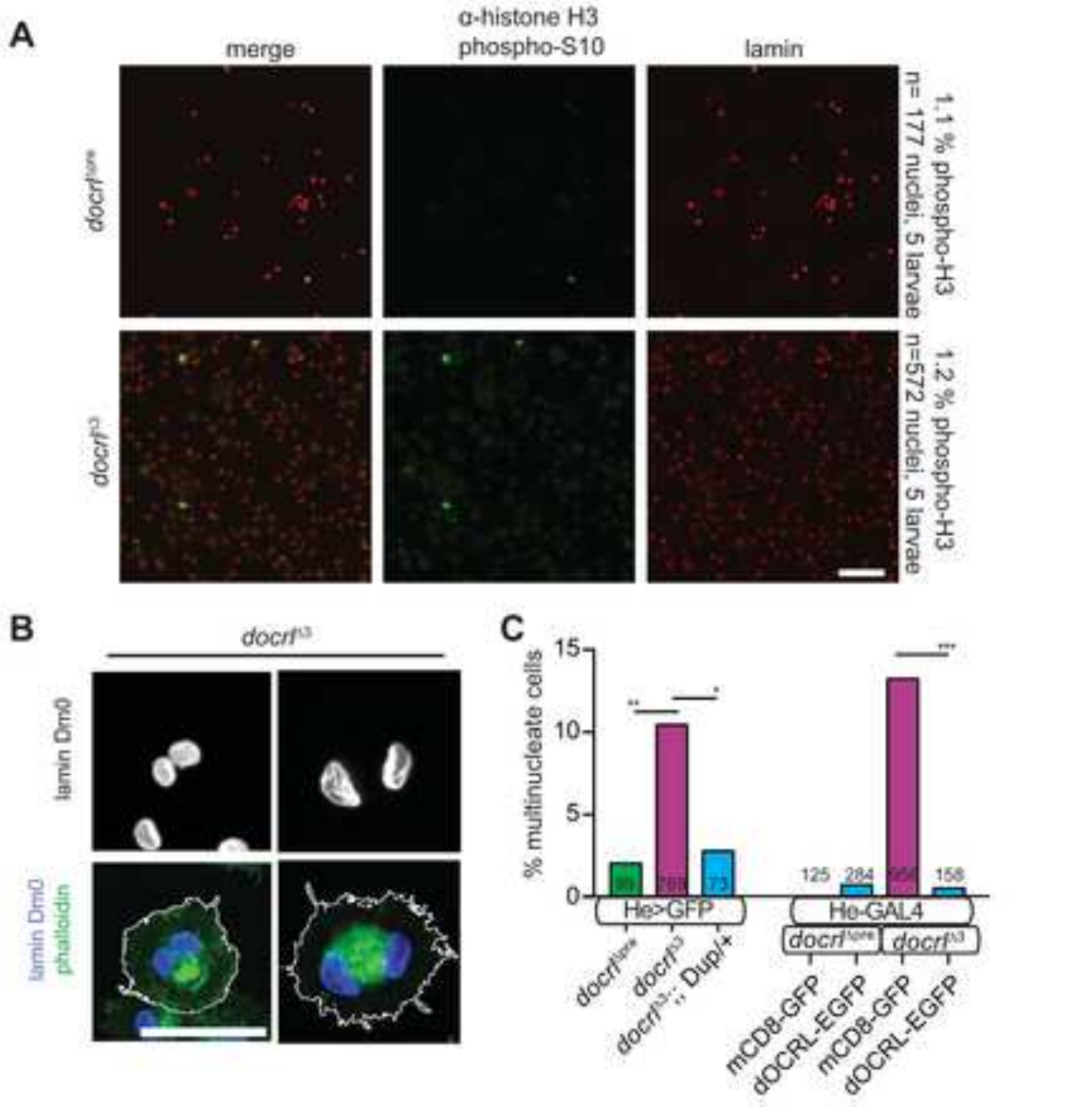

Figure S3

Click here to download Figure FigS3.tiff

Del Signore et al., Figure S3

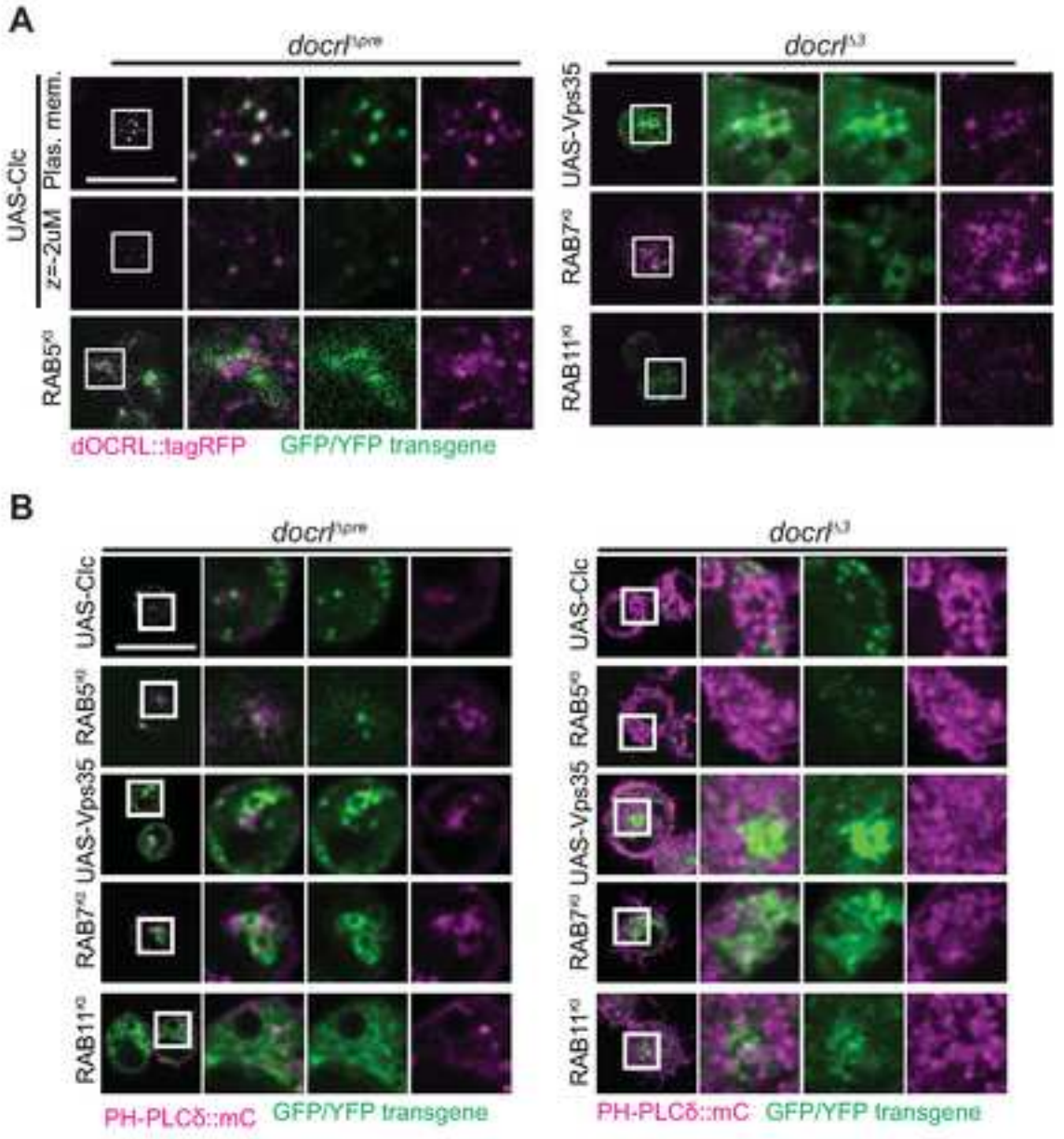

Figure S4

Click here to download Figure FigS4.tiff

Del Signore et al., Figure S4

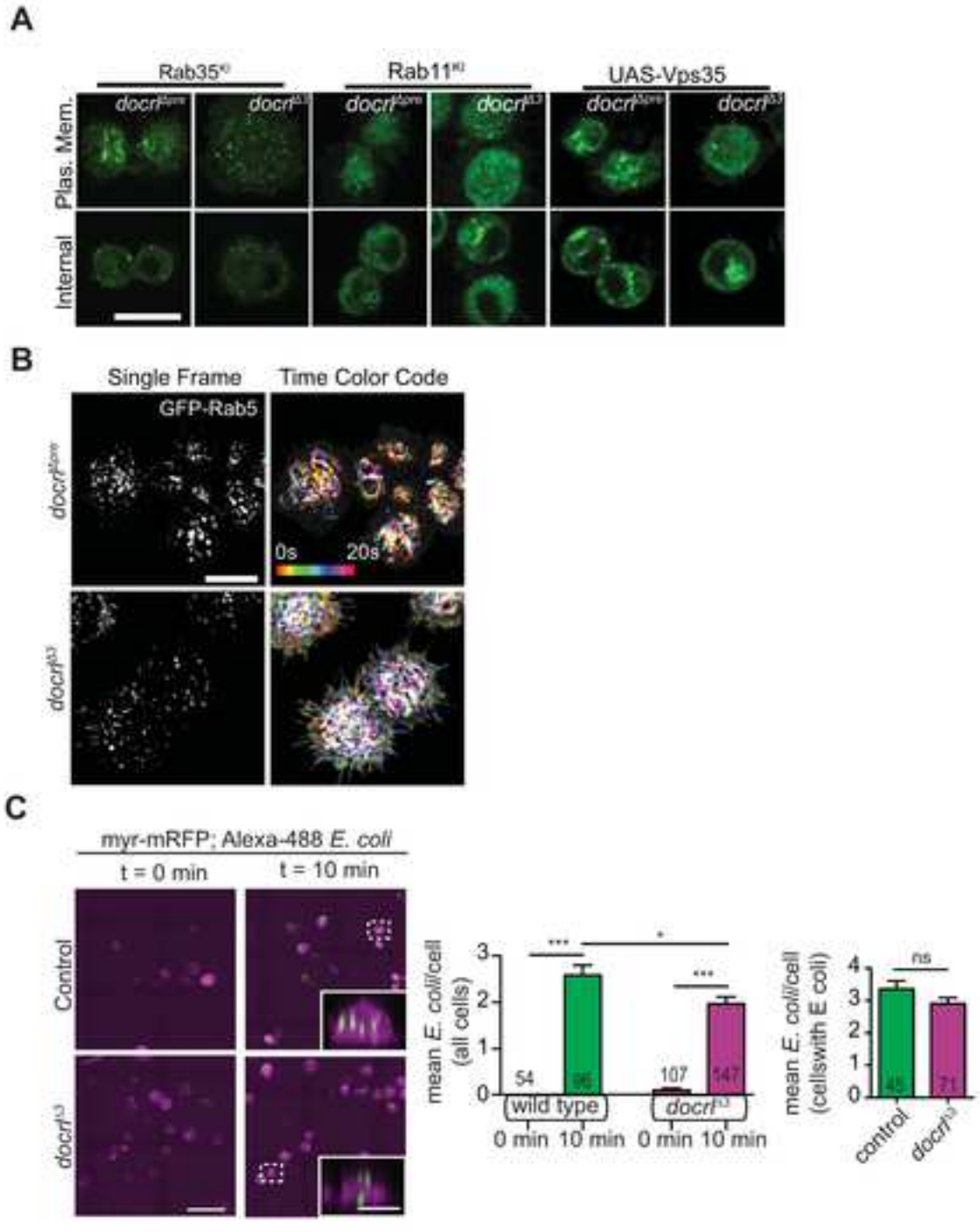

Figure S5

Click here to download Figure FigS5.tiff

Del Signore et al., Figure S5

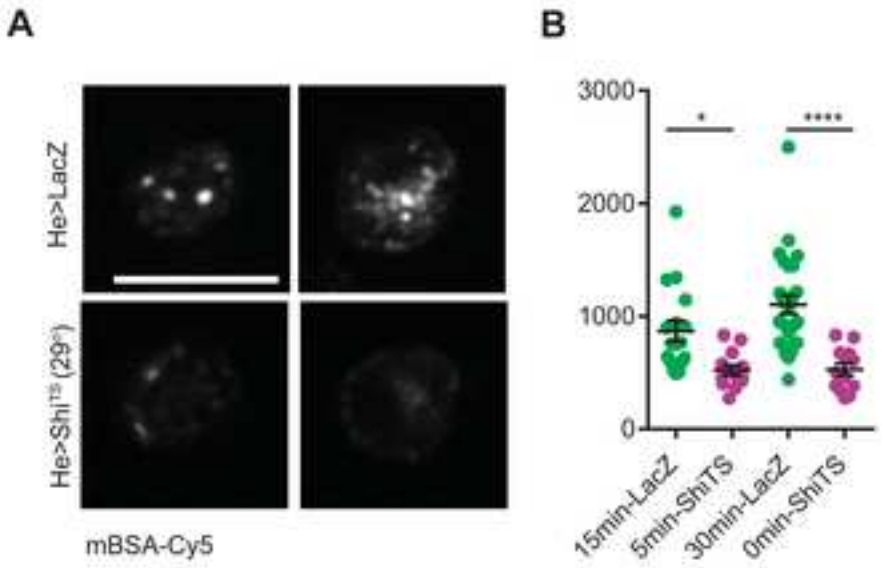

Figure S6

Click here to download Figure FigS6.tiff

Del Signore et al., Figure S6